

Point-Based Manifold Harmonics

Abstract—This paper proposes an algorithm to build a set of orthogonal Point-Based Manifold Harmonic Bases (PB-MHB) for spectral analysis over point-sampled manifold surfaces. To ensure that PB-MHB are orthogonal to each other, it is necessary to have symmetric discrete Laplace-Beltrami Operator (LBO) over the surfaces. Existing converging discrete LBO proposed by Belkin *et al* [1] is not guaranteed to be symmetric. We build a new point-wisely discrete LBO over the point-sampled surface that is guaranteed to be symmetric, and prove its convergence. By solving the eigen problem related to the new operator, we define a set of orthogonal bases over the point cloud. Experiments show that the new operator is converging better than other symmetric discrete Laplacian operators (such as graph Laplacian) defined on point-sampled surfaces, and can provide orthogonal bases for further spectral geometric analysis and processing tasks.

Index Terms—Point-Sampled Surface, Laplace-Beltrami Operator, Eigen Function

I. INTRODUCTION

A. Background

In computer image processing, spectral methods like Discrete Cosine Transform and Fourier Transform are widely used for analyzing signals. In geometric processing, however, spectral method is not well developed [2] as compared to image processing, because it is more difficult to define the Laplace-Beltrami operator on arbitrarily discretized shapes.

Laplace operator Δ is a simple second-order differential operator (the divergence of gradient) defined in Euclidean space \mathbb{R}^n . Similarly, we can define the Laplace-Beltrami Operator (LBO) in the closed n -dimensional Riemannian manifold \mathcal{M} as the divergence of gradient:

$$\begin{aligned} \Delta_{\mathcal{M}}f &= \text{div grad } f \\ &= \frac{1}{\sqrt{|g|}} \sum_i \partial_i \left(\sum_j \sqrt{|g|} g^{ij} \partial_j f \right), \end{aligned} \quad (I.1)$$

where g is the metric tensor over the manifold \mathcal{M} , g_{ij} is the element of g , g^{ij} is the element of g^{-1} . The eigen problem of LBO can be defined as:

$$\Delta_{\mathcal{M}}H = -\lambda H, \quad (I.2)$$

where λ and H are the eigen-value and corresponding eigen-function (also called eigen-vector in discrete form). Here the minus sign “-” is used to ensure that all $\lambda \geq 0$. Note that some researchers [3] define $\Delta_{\mathcal{M}} = -\text{div grad}$, in which case the minus sign in equation (I.2) can be removed. From now on we will denote the i -th eigen-value and the corresponding eigen-function (eigen-vector) as λ_i and H^i .

Continuous LBO is a symmetric operator:

$$f \cdot \Delta_{\mathcal{M}}g = - \int_{\mathcal{M}} \langle \nabla f, \nabla g \rangle \quad (I.3)$$

$$= \Delta_{\mathcal{M}}f \cdot g. \quad (I.4)$$

Here f and g are functions defined over the manifold surface, ∇ denotes the gradient operator. With this property, we know

that eigen-functions with different eigen-values are orthogonal to each other:

$$H^i \cdot \Delta_{\mathcal{M}}H^j = \lambda_i H^i \cdot H^j = \lambda_j H^i \cdot H^j \quad (I.5)$$

$$\text{if } \lambda_i \neq \lambda_j \quad (I.6)$$

$$H^i \cdot H^j = 0. \quad (I.7)$$

Note that constant functions with $\lambda = 0$ is a solution for any Laplacian operator. We denote $\lambda_0 = 0$ with corresponding eigen-function $H^0 = \text{constant}$. Other eigen-values are sorted according to their magnitudes: $0 = \lambda_0 \leq \lambda_1 \leq \lambda_2 \leq \dots$.

With the development of 3D scanning technology, it is much easier to generate 3D models from real objects today. For most of these surfaces we only have discrete representations such as polygonal meshes or point clouds. Thus we need to define the discrete form of LBO over the discrete representation of surfaces to perform the geometric analysis. By solving the above eigen problem, we can get a set of eigen-vectors $\{H^i\}$ defined over the discrete manifold surfaces [4]. Different eigen-vectors corresponding to different eigen-values are orthogonal to each other. These vectors are called the Manifold Harmonic Bases (MHB), and they have been used for spectral analysis over triangle mesh surfaces [5].

B. Motivation and Contribution

As a discrete representation of surfaces, the point cloud is less explored, comparing with polygonal meshes. The 3D scanning devices can produce point clouds sampled from object surfaces easily. Comparing with mesh, point clouds do not provide any information about the connectivity. This makes point clouds more difficult to process than meshes. Because the Laplacian operator employed in Manifold Harmonics proposed by Vallet *et al* [5] requires the connectivity information, it can not be applied to point clouds directly. This paper extends the Manifold Harmonics framework to the geometry processing of point clouds.

Belkin *et al* [1] proposed a novel method to compute the discrete LBO on manifolds represented by point clouds. They also proved that this discrete LBO denoted as L_P^t is converging as points get denser. However, their discrete LBO is not guaranteed to be symmetric. It is important for discrete LBO to be symmetric in Manifold Harmonics because symmetric operator is guaranteed to provide orthogonal bases. For non-symmetric matrix operator L , if it can be decomposed as $L = B^{-1}Q$ where Q is symmetric and B is diagonal, it is a widely-used technique to compute the generalized eigen problem $Qx = -\lambda Bx$ instead of the standard eigen problem $Lx = -\lambda x$ [4]. With a modified definition of inner product $\langle x, y \rangle = x^T B y$, it is still possible to ensure orthogonality of the eigen-vectors. But as shown in Figure 1(a), Belkin *et al*'s LBO L_P^t is trying to compute the integration over the estimated tangent planes via local triangulations. Each point is assigned a different “weight” for the computations on the

tangential spaces of its neighboring points. Thus L_P^t can not be decomposed into multiplication of diagonal matrix B^{-1} and symmetric matrix Q . Using $(L_P^t + (L_P^t)^T)/2$ instead of L_P^t is a trivial extension to make it symmetric. Lévy [6] used this technique with cotangent weighted graph Laplacian. But our experiments in section V show that this trivial extension does not converge.

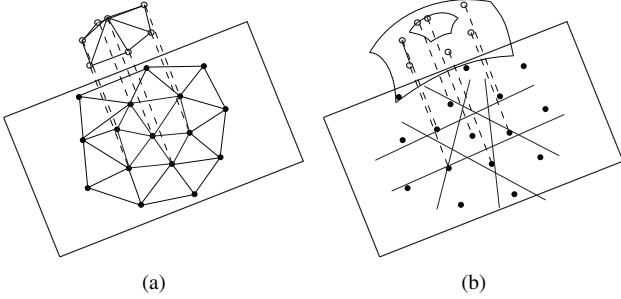


Fig. 1. (a) Belkin *et al*'s approach [1]: integration over the estimated tangent plane in L_P^t ; (b) our approach: integration over the manifold with Voronoi cell computation on the estimated tangent plane in \hat{L}_P^t .

To ensure that the bases $\{H^i\}$ are orthogonal to each other, we propose a new method to construct the symmetric discrete LBO \hat{L}_P^t over point clouds sampled from manifold surfaces. We also prove that this new operator is converging as point clouds get denser and satisfy certain sampling conditions. Based on the symmetric property of this new operator, we can construct a set of point-wisely converging manifold harmonic bases, to be used for general spectral analysis over the point-sampled surfaces. We summarize the contributions of this paper as follows:

- 1) We propose a provable construction algorithm for the *symmetric* and *converging* Laplace-Beltrami operator over point-sampled manifold surfaces based on computing the integration over the manifolds numerically. The symmetric property of LBO, resulted from our local Voronoi computation, guarantees the orthogonality of the computed Point-Based Manifold Harmonic Bases (PB-MHB). The construction process based on the heat diffusion kernel guarantees the convergence of the discretized LBO (Theorem 4.11), and leads to more accurate manifold harmonic bases.
- 2) Our algorithm can be directly applied to the point clouds using a local Voronoi computation procedure in the tangential space (Figure 1(b)), based on our theoretical proof that the estimated Voronoi cell area on the tangential space is converging to its counterpart on the manifold (Theorem 4.6), as long as the point clouds satisfy certain sampling condition (addressed in section III-A). So we do not need a global mesh for the manifold surface to compute the orthogonal bases.
- 3) The experimental results shown in section V are very encouraging. The convergence of our new LBO is better than other point-based symmetric discrete Laplace operators, such as the graph Laplacian, or the trivial extension of Belkin *et al*'s operator $(L_P^t + (L_P^t)^T)/2$. The computed orthogonal bases are also performing

better for general geometric processing tasks such as spectral filtering which can be used to smooth models or to enhance details.

II. RELATED WORK

Researchers have been looking for spectral geometric processing methods [2], [7], for surface smoothing [8], segmentation [9], compression [10], watermarking [11], [12], quadrangulation [13], [14], conformal parameterization [15], matching and retrieval [4], [16], etc. Manifold Harmonics, as proposed by Vallet *et al* [5], is defined as the eigenfunctions of LBO, based on the Discrete Exterior Calculus (DEC) computational framework.

Discretizing Laplacian operator on mesh surfaces is an active research area. Most of the proposed discretization methods [8], [17], [18], [19] applied finite element methods with different assumptions. They have similar forms of *cotangent scheme* [20] despite those different assumptions. Xu [19] gave a theoretical analysis of the available discrete LBOs defined on meshes about their convergence property. It shows that the cotangent scheme does not converge to the continuous counterpart in general, except for the versions in Desbrun *et al* [17] and Meyer *et al* [18] applied to some special classes of meshes, such as certain meshes with valence 6. Hildebrandt *et al* [21] analyzed the convergence of LBO and showed that the cotangent scheme has weak convergence for the solution of the Dirichlet's problem, assuming the aspect ratios of the triangles are bounded. A recent work by Wardetzky *et al* [22] showed that a "perfect" discrete LBO based on mesh connectivity satisfying all the properties of the continuous one cannot exist on general meshes. Reuter *et al* [23] showed that their discrete LBO based on cubic FEM works very well with respect to the continuous case, and demonstrated the applications in shape understanding.

Rosenberg [3] suggested the relationship between the LBO and the heat equation on manifolds. Belkin *et al* [24] extended this method by proving that it is possible to approximate LBO on the estimated tangent planes of surfaces with the Gaussian kernel. They [25] proposed the first algorithm for approximating the LBO of a surface from a mesh with point-wise convergence guarantees. This method was extended later [1] to discretize LBO on manifold surfaces represented as point clouds. Their matrix form LBO [1], denoted as L_P^t , has been proved to converge point-wisely as point clouds get denser. However, their discrete LBO on the point cloud is not guaranteed to be symmetric, which cannot be used for computing the orthogonal bases on surfaces. LBO is naturally related to diffusion [26], which is also used in dimensional reduction and other applications.

Due to the lack of connectivity information, computing LBO on the point cloud is traditionally carried out in the local neighborhood of each point, by the combinatorial graph Laplacian [27], [11], which is hard to be geometry-aware. Since LBO is a differential operator, computing LBO on the point cloud is closely related to the integral computation on point clouds. Luo *et al* [28] worked on integral estimation over manifolds represented by point clouds. They employed

the Voronoi diagrams based on the geodesic distance while our paper uses the Euclidean distance. We choose Euclidean Voronoi diagrams because it provides (1) the convergence rate of $O(\varepsilon^2)$ rather than $O(\varepsilon)$ of geodesic Voronoi diagrams, with the specific sampling condition ε defined in definition 3.1; and (2) bounding properties on both Voronoi cells (Lemma 4.1) and Voronoi neighbors (Lemma 4.2) that ease the proof of Lemma 4.10 which is the key to the proof of the final convergence property of our LBO in Theorem 4.11. We estimate the area of the Euclidean Voronoi cell on the local tangent plane, and prove its convergence in section IV-A. The convergence proof in this paper is dependent on some geometric properties of point clouds, which have been studied in the literature of surface reconstruction and computational geometry [29], [30], [31], [32].

III. CONSTRUCTION OF PB-MHB

A. Definitions

To construct the discrete LBO, the point clouds need to satisfy some sampling conditions defined as follows:

Definition 3.1 (Sampling Condition): Let $\varepsilon > 0$. A finite sample $P \subset \mathcal{M}$ is called an ε -sample if

$$\forall x \in \mathcal{M}, \exists p \in P : \|x - p\| \leq \varepsilon. \quad (\text{III.1})$$

And the ε -sample P is called an (ε, ζ) -sample or tight ε -sample if it satisfies the additional condition:

$$\forall p, q \in P : \|p - q\| \geq \zeta, \quad (\text{III.2})$$

where $\varepsilon > \zeta > 0$.

It is obvious that any (ε, ζ) -sample is also an ε -sample.

In this paper, we assumed that the given point cloud P is an $(\varepsilon, s\varepsilon)$ -sample of the manifold \mathcal{M} . $0 < s < 1$ is a fixed positive number for the given point cloud P . That is, any two points in P can not be extremely close. This property is used to ensure that the estimation of the Voronoi cells described in section III-B is converging, which is proved in section IV-A. We will employ Voronoi cells on manifolds in the construction process of discrete LBO. The Voronoi cell of a point p on manifold is the intersection of \mathcal{M} and the Voronoi cell of p in Euclidean space \mathbb{R}^3 . We define the Voronoi cells on manifolds as follows:

Definition 3.2 (Voronoi Cell): For the point set P sampled on the manifold \mathcal{M} , the Voronoi cell of a point $p \in P$ on \mathcal{M} is defined as the subset of \mathcal{M} :

$$Vr_{\mathcal{M}}(p) = \{q | q \in \mathcal{M}, \forall p' \in P, p' \neq p, \|q - p\| \leq \|q - p'\|\},$$

where $\|q - p\|$ stands for the Euclidean distance between points p and q .

We also need to use the Local Feature Size to characterize how much the manifold \mathcal{M} bends locally at a given point. The larger the feature size, the flatter the surface is. Local Feature Size is used in the proof of error bound in section IV. Its definition is related to the Medial Axis of \mathcal{M} :

Definition 3.3 (Medial Axis): A ball B is called a medial ball of \mathcal{M} , if B does not contain any point of \mathcal{M} in its interior but at least two points of \mathcal{M} on its boundary. The medial axis

of \mathcal{M} is the closure of the set of all midpoints of the medial balls.

Definition 3.4 (Local Feature Size): The local feature size is the function $\rho : \mathcal{M} \rightarrow \mathbb{R}$ that assigns to $x \in \mathcal{M}$ its distance to the medial axis.

In this paper the local feature size $\rho(p)$ of a specific point p is referred as ρ to simplify the notation.

B. Computing the Approximation of $\Delta_{\mathcal{M}}f(p)$

To build a discrete LBO approximating the continuous LBO $\Delta_{\mathcal{M}}$ on the point-sampled surfaces, it is necessary to approximate $\Delta_{\mathcal{M}}f(p)$ one by one for all points $p \in P$. Following is the algorithm to approximate $\Delta_{\mathcal{M}}f(p)$:

- 1) Tangent Plane Estimation: Set $r = 10\varepsilon$ [1], where the point cloud P is ε -sampled. Here 10ε is used to ensure that the estimated tangent plane is converging to the real tangent plane, which is proved in Belkin *et al*'s paper [1]. Consider the point set $P_r \subseteq P$ within distance r away from p , i.e., $P_r = P \cap B(p, r)$ where $B(p, r)$ is the ball centered at p with radius r . Let Q^* be the best fitting plane passing through p such that $d(P_r, Q^*)$ is minimized. Using Har-Peled and Varadarajan's algorithm [33] (also used by Belkin *et al* [1]), we construct a 2-approximation \hat{T}_p of Q^* , i.e., \hat{T}_p is a plane passing through p , and $d_H(P_r, \hat{T}_p) \leq 2d_H(P_r, Q^*)$, where $d_H(\cdot, \cdot)$ is the Hausdorff distance.
- 2) Voronoi Cell Estimation: Fix a positive constant $\delta \geq 10\varepsilon$, and consider the set of points P_δ that are within δ away from p , i.e., $P_\delta = P \cap B(p, \delta)$. Here $\delta \geq 10\varepsilon$ is to ensure we have enough local neighboring points for approximation. We project the points in P_δ to \hat{T}_p . When δ is sufficiently small, this projection is bijective. We denote the projection as $\hat{\Pi}$. Then we build the Voronoi Diagram of $\hat{\Pi}(P_\delta)$ on \hat{T}_p . Take the area of the Voronoi cell $Vr_{\hat{T}_p}(p)$ on \hat{T}_p as an approximation of the Voronoi cell area of p on surface, $Vr_{\mathcal{M}}(p)$. $Vr_{\hat{T}_p}(p)$ is also denoted as $Vr_{\hat{T}}(p)$ in this paper to simplify the notation. When the point cloud P gets denser, the area of $Vr_{\hat{T}}(p)$ is converging to the area of $Vr_{\mathcal{M}}(p)$, which is proved in section IV-A.
- 3) Integration Approximation: We compute $\Delta_P^t f(p)$ as an approximation to $\Delta_{\mathcal{M}}f(p)$ as follows:

$$\Delta_P^t f(p) = \frac{1}{4\pi t^2} \sum_{q \in P_\delta} (e^{-\frac{\|q-p\|^2}{4t}} (f(q) - f(p)) \text{vol}(Vr_{\hat{T}}(q))). \quad (\text{III.3})$$

Here $\text{vol}(\cdot)$ denotes the area of the given Voronoi cell. $Vr_{\hat{T}}(q)$ is the Voronoi cell of point q in its own estimated tangent plane \hat{T}_q . Because the new operator is defined on the point cloud P and employs the parameter t , here we denote it as Δ_P^t . Similar to Belkin *et al*'s method [1], $t(\varepsilon) = \varepsilon^{\frac{1}{2+\xi}}$, and $\xi > 0$ is an arbitrary selected positive fixed number, used to ensure the convergence of Δ_P^t . We are employing the Gaussian kernel to approximate the heat function locally on the manifold \mathcal{M} , and t is the "time" of the heat diffusion process. In section IV-B, we prove that as the points get denser, Δ_P^t

will converge to $\Delta_{\mathcal{M}}$ (Theorem 4.11). In the following section III-C, we assemble Δ_P^t into its matrix form \hat{L}_P^t .

C. Construction of the LBO in Matrix Form

For continuous LBO, since $f \cdot \Delta_{\mathcal{M}} g = \Delta_{\mathcal{M}} f \cdot g$ holds, $\Delta_{\mathcal{M}}$ is symmetric. Correspondingly in the discrete case, we expect $\mathbf{f}^T L \mathbf{g} = (L \mathbf{f})^T \mathbf{g}$ holds, where L is any discrete LBO in its matrix form. Thus, we expect $L = L^T$, which means that the discrete LBO matrix L should be symmetric.

Belkin *et al* claimed that their discrete LBO matrix L_P^t [1] is converging point-wisely. However, their L_P^t is not guaranteed to be symmetric. In our application, to build the orthogonal Manifold Harmonic Bases, it is necessary to have symmetric discrete Laplacian operator. A trivial way is to use $(L_P^t + (L_P^t)^T)/2$ instead of L_P^t . However, our experiments in section V show that this trivial extension does not converge at all.

In our method, we build the discrete LBO Δ_P^t from the equation (III.3) which is linear on the function values $f(p_i)$, for $p_i \in P$. Thus it can be written as $\Delta_P^t f(p_i) = \hat{R}_i^T \mathbf{f}$, where \hat{R}_i is an N -vector, $\mathbf{f} = [f(p_1), f(p_2), \dots, f(p_N)]^T$ is the N -vector representing the input continuous function f sampled at the points, and $N = |P|$. Thus we have the matrix form \hat{L}_P^t of our discrete LBO Δ_P^t over the point cloud:

$$\Delta_P^t f = \hat{L}_P^t \cdot \mathbf{f}, \quad (\text{III.4})$$

where \hat{R}_i^T is the i -th row of matrix \hat{L}_P^t . We can rewrite the matrix form as $\hat{L}_P^t = B^{-1} \cdot Q$, where the elements q_{ij} of the symmetric matrix Q , and the diagonal elements b_{ii} of the diagonal matrix B can be computed as follows:

$$q_{ij} = \text{vol}(Vr_{\hat{T}}(p_i)) \text{vol}(Vr_{\hat{T}}(p_j)) \frac{1}{4\pi t^2} e^{-\frac{\|p_i - p_j\|^2}{4t}}, \quad (\text{III.5})$$

$$\text{where } i \neq j, \quad \|p_i - p_j\| \leq \delta,$$

$$\text{and } t(\varepsilon) = \varepsilon^{\frac{1}{2+\varepsilon}}, \quad \varepsilon > 0,$$

$$q_{ii} = - \sum_{j \neq i} q_{ij}, \quad (\text{III.6})$$

$$b_{ii} = \text{vol}(Vr_{\hat{T}}(p_i)). \quad (\text{III.7})$$

By redefining the functional inner product in matrix form as $\langle \mathbf{f}, \mathbf{g} \rangle = \mathbf{f}^T B \mathbf{g}$, we have:

$$\begin{aligned} \langle \mathbf{f}, \hat{L}_P^t \mathbf{g} \rangle &= \mathbf{f}^T B (B^{-1} Q \mathbf{g}) \\ &= \mathbf{f}^T Q \mathbf{g} \\ &= \mathbf{f}^T Q^T (B B^{-1})^T \mathbf{g} \\ &= (B^{-1} Q \mathbf{f})^T B \mathbf{g} \\ &= \langle \hat{L}_P^t \mathbf{f}, \mathbf{g} \rangle, \end{aligned}$$

which means we have the symmetric operator \hat{L}_P^t now.

D. Point-Based Manifold Harmonic Transform

Having the symmetric LBO matrix operator $\hat{L}_P^t = B^{-1} \cdot Q$, we can solve the following generalized eigen problem:

$$Q \mathbf{H} = -\lambda B \mathbf{H}. \quad (\text{III.8})$$

By solving this problem, we have eigen-values $\{\lambda_i\}$ and corresponding eigen-vectors $\{H^i\}$. $\{H^i\}$ are called the *Point-Based Manifold Harmonic Bases* (PB-MHB) of the sampled

manifold surface. PB-MHB can be used for the general spectral processing of 3D models.

Without any loss of generality, we assume that all the eigen-vectors are normalized $\langle H^i, H^i \rangle = (H^i)^T B H^i = 1$, and $\lambda_i \leq \lambda_j$ holds for all $i < j$. Because $\langle H^i, H^j \rangle = (H^i)^T B H^j = \delta_{ij}$ holds where δ_{ij} is Kronecker delta, the eigen-vectors $\{H^i\}$ can be used in Fourier-like spectral decomposition for functions defined over point-sampled manifold surfaces:

$$\tilde{f}_i = \langle \mathbf{f}, H^i \rangle = \mathbf{f}^T B H^i, \quad (\text{III.9})$$

where \mathbf{f} is the vector of function values sampled on the point cloud. This process is called *Point-Based Manifold Harmonic Transform* (PB-MHT). With $\{\tilde{f}_i\}$, we can reconstruct \mathbf{f} using the Inverse PB-MHT:

$$\mathbf{f} = \sum \tilde{f}_i \cdot H^i \quad (\text{III.10})$$

We can consider the coordinates of the points as three continuous functions defined over the manifold surface: \mathbf{x} , \mathbf{y} and \mathbf{z} . By employing PB-MHT presented above, we can decompose the manifold surface into its spectral representation $(\tilde{x}_i, \tilde{y}_i, \tilde{z}_i)$ and recover them using the Inverse PB-MHT. In section V we show the results of applying some spectral filters on general point-sampled surfaces, by modifying their spectral representations $\{\tilde{x}_i, \tilde{y}_i, \tilde{z}_i\}$. Figure 2 shows the results of applying two spectral filters on the point-sampled Chinese Lion model. This can be used to remove noises from scanned surfaces or to enhance detailed features.

IV. CONVERGENCE PROOF

In our construction of PB-MHB, the assumption is we have a continuous closed differentiable Riemannian manifold \mathcal{M} on which the sample set P lies. f is a C^2 continuous function defined over \mathcal{M} . We are going to prove that the result of our discrete LBO applied on the function $\hat{L}_P^t \mathbf{f}$ converges to the continuous result $\Delta_{\mathcal{M}} f$ point-wisely.

To show the convergence of \hat{L}_P^t , first we are proving that our estimation of the Voronoi cell area is converging to the real Voronoi cell area as point clouds get denser. This part is proved in section IV-A. After having the Voronoi cell area convergence result, we prove that $\hat{L}_P^t \mathbf{f}$ converges to $\Delta_{\mathcal{M}} f$ point-wisely in section IV-B.

A. Convergence of Estimated Voronoi Cell Area

Since we employ the estimated area of the Voronoi cell $\text{vol}(Vr_{\hat{T}}(p))$ on the tangential space, instead of the area of the real Voronoi cell $\text{vol}(Vr_{\mathcal{M}}(p))$ on the manifold, to approximate the integration over manifold surfaces, it is important to make sure this estimation is converging. To establish this result, we go through the following two steps: (1) we prove that the projection of $Vr_{\mathcal{M}}(p)$ on the estimated tangent plane \hat{T}_p , $\hat{\Pi}(Vr_{\mathcal{M}}(p))$, has converging area to $Vr_{\mathcal{M}}(p)$, as shown in Lemma 4.5; (2) we build the converging upper bound and the lower bound of $\text{vol}(\hat{\Pi}(Vr_{\mathcal{M}}(p)))$ that are both converging to $\text{vol}(Vr_{\hat{T}}(p))$. By combining these two results, we can prove the convergence of $\text{vol}(Vr_{\hat{T}}(p))$ to $\text{vol}(Vr_{\mathcal{M}}(p))$, as shown in Theorem 4.6.

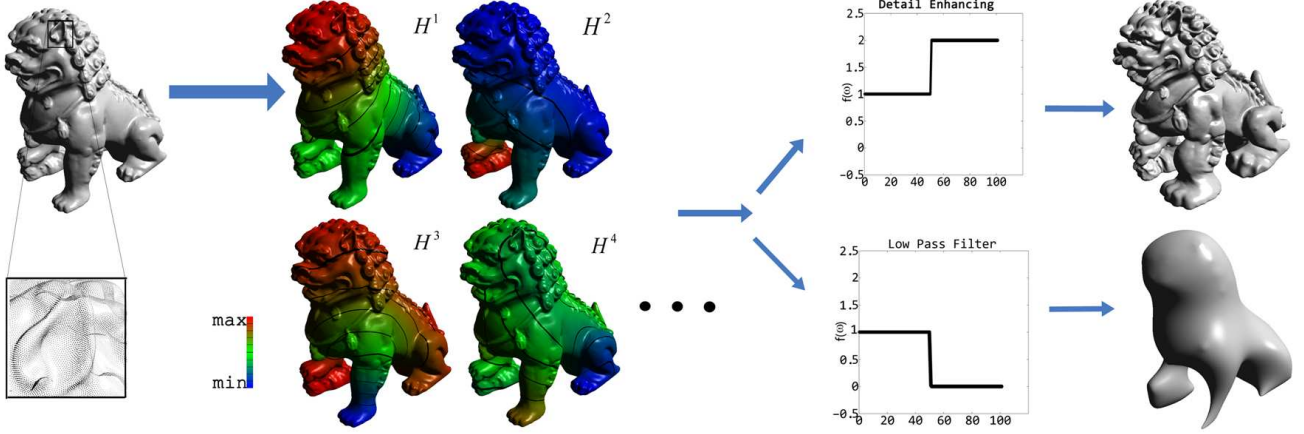


Fig. 2. From left to right: the point-sampled Chinese Lion, H^1 to H^4 bases, and two filtering results.

To begin with the above first step, we need to prove that given the assumption of P being ε -sampled, there are some bounds on the sizes of the Voronoi cells $Vr_{\mathcal{M}}(p)$ and $Vr_{\hat{T}_p}(p)$ (Lemma 4.1 and Lemma 4.3), and there are some bounds on the set of neighboring points that may influence these Voronoi cells (Lemma 4.2 and Lemma 4.4).

Lemma 4.1 (Bound of $Vr_{\mathcal{M}}(p)$): Consider the underlying manifold \mathcal{M} and its ε -sampling P , for $\forall p \in P$:

$$Vr_{\mathcal{M}}(p) \subseteq B(p, \varepsilon) \quad (\text{IV.1})$$

holds, i.e., its Voronoi cell on the manifold is bounded by a ball with radius ε .

Proof: Suppose $\exists q \in Vr_{\mathcal{M}}(p) \subseteq \mathcal{M}$, that satisfies $\|p - q\| > \varepsilon$.

$\therefore P$ is ε -sampling,

\therefore There is another point $p' \in P$ that satisfies $\|p' - q\| \leq \varepsilon < \|p - q\|$, which means q is closer to p' instead of p .

$\therefore q \notin Vr_{\mathcal{M}}(p)$. This is contradictory to assumption. ■

Lemma 4.2 (Bound of Influencing Points on \mathcal{M}):

Consider the boundary of the Voronoi cell: $\partial Vr_{\mathcal{M}}(p)$. Given that P is an ε -sampling of \mathcal{M} , for $\forall q \in \partial Vr_{\mathcal{M}}(p)$, there is some point $\exists p' \in P$ satisfies $\|q - p\| = \|q - p'\|$, then for all such kind of points p' ,

$$\|p - p'\| \leq 2\varepsilon \quad (\text{IV.2})$$

holds. That is, only the point set in $B(p, 2\varepsilon)$ may influence the Voronoi cell of point p .

Proof: According to Lemma 4.1, we have $\|q - p\| \leq \varepsilon$ and $\|q - p'\| \leq \varepsilon$ hold for $\forall q \in \partial Vr_{\mathcal{M}}(p)$. Thus we have

$$\|p - p'\| \leq \|q - p\| + \|q - p'\| \leq \varepsilon + \varepsilon = 2\varepsilon. \quad (\text{IV.3})$$

As described in section III-B, we project a local neighborhood of points $P_\delta = P \cap B(p, \delta)$, $\delta \geq 10\varepsilon$ onto the estimated tangent plane \hat{T}_p . When δ , ε and $r/\rho = 10\varepsilon/\rho$ are small enough, the projection from the local patch $\mathcal{M} \cap B(p, \delta)$ to \hat{T}_p , denoted as $\hat{\Pi}$, is bijective. Let $\hat{\Phi} = \hat{\Pi}^{-1}$.

Lemma 4.3 (Bound of $Vr_{\hat{T}_p}(p)$): Consider the Voronoi diagram of $p \cup \{\hat{\Pi}(P_\delta - p)\}$ on \hat{T}_p , where $p \in P$ is a sample

point and P is an ε -sampling of \mathcal{M} . Denote the Voronoi cell of p on \hat{T}_p as $Vr_{\hat{T}_p}(p)$, then

$$Vr_{\hat{T}_p}(p) \subseteq B(p, \varepsilon) \quad (\text{IV.4})$$

holds when ε is small enough. That is, $Vr_{\hat{T}_p}(p)$ is bounded by a ball with radius ε .

Proof:

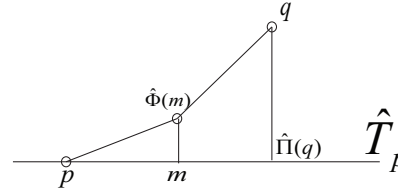


Fig. 3. Bound of $Vr_{\hat{T}_p}(p)$ for Lemma 4.3.

Suppose $\exists m \in Vr_{\hat{T}_p}(p)$ and $\|p - m\| > \varepsilon$, as shown in Figure 3, $\hat{\Phi}(m) \in \mathcal{M}$. Because $Vr_{\hat{T}_p}(p)$ is convex, without losing generality, we can assume $\varepsilon < \|p - m\| < 2\varepsilon$.

When ε is small enough, we have $(\hat{T}_p \cap B(p, 3\varepsilon)) \subseteq \hat{\Pi}(\mathcal{M} \cap B(p, \delta))$.

Here $p = \hat{\Pi}(p)$ since p lies on both \mathcal{M} and \hat{T}_p .

$\therefore \hat{\Pi}$ is the projection from \mathcal{M} to \hat{T}_p and $\hat{\Phi} = \hat{\Pi}^{-1}$,

$\therefore \|p - \hat{\Phi}(m)\| \geq \|p - m\| > \varepsilon$,

$\therefore P$ is ε -sample of \mathcal{M} ,

$\therefore \exists q \in P$, $p \neq q$, $\|m - \hat{\Pi}(q)\| \leq \|q - \hat{\Phi}(m)\| < \varepsilon$,

$\therefore \|p - q\| \leq \|p - m\| + \|m - \hat{\Pi}(q)\| < 3\varepsilon$,

$\therefore q \in P_\delta$ since $(\hat{T}_p \cap B(p, 3\varepsilon)) \subseteq \hat{\Pi}(\mathcal{M} \cap B(p, \delta))$.

$\therefore m \in Vr_{\hat{T}_p}(q)$, $m \notin Vr_{\hat{T}_p}(p)$. This is contradictory to the assumption. ■

Lemma 4.4 (Bound of Influencing Points on \hat{T}_p):

Consider the boundary of the Voronoi cell on the estimated tangent plane: $\partial Vr_{\hat{T}_p}(p)$. Given that P is an ε -sampling of \mathcal{M} , for $\forall q \in \partial Vr_{\hat{T}_p}(p)$, there is some point $\exists p' \in P$ satisfies $\|q - p\| = \|q - \hat{\Pi}(p')\|$, then for all such kind of points p' ,

$$\|p - \hat{\Pi}(p')\| \leq 2\varepsilon \quad (\text{IV.5})$$

holds when ε is small enough. That is, only the projected sample points in $B(p, 2\varepsilon)$ may influence the Voronoi cell $Vr_{\hat{T}_p}(p)$.

Proof: According to Lemma 4.3, we know that

$$\forall q \in \partial Vr_{\hat{T}_p}(p), \|p - q\| \leq \varepsilon.$$

Thus for the influencing projected point $\hat{\Pi}(p')$ we have

$$\|p - q\| = \|q - \hat{\Pi}(p')\| \quad (\text{IV.6})$$

$$\|p - \hat{\Pi}(p')\| \leq \|p - q\| + \|q - \hat{\Pi}(p')\| \quad (\text{IV.7})$$

$$\leq \varepsilon + \varepsilon = 2\varepsilon \quad (\text{IV.8})$$

Lemma 4.5 (Convergence of $\hat{\Pi}(Vr_{\mathcal{M}}(p))$ to $Vr_{\mathcal{M}}(p)$):

Consider projecting $Vr_{\mathcal{M}}(p)$ to \hat{T}_p . P is an ε -sampling of \mathcal{M} , and ρ is the local feature size of point $p \in P$. Then

$$\left\| \frac{\text{vol}(Vr_{\mathcal{M}}(p))}{\text{vol}(\hat{\Pi}(Vr_{\mathcal{M}}(p)))} - 1 \right\| = O\left(\frac{\varepsilon^2}{\rho^2}\right) \quad (\text{IV.9})$$

holds.

Proof:

$\forall q \in Vr_{\mathcal{M}}(p)$, consider the angle $\angle(T_q, \hat{T}_p)$ between the two planes T_q and \hat{T}_p , where T_p and T_q are the real tangent planes of \mathcal{M} at points p and q , \hat{T}_p is the estimated tangent plane at point p , as described in section III-B.

According to Lemma A.1 (in appendix A), when $\|p - q\| < \rho/3$ we have

$$\angle(T_p, T_q) \leq \frac{\|p - q\|}{\rho - \|p - q\|} \leq O(\varepsilon/\rho). \quad (\text{IV.10})$$

We get the last inequality by applying Lemma 4.1.

Now we have three planes here: T_p , T_q and \hat{T}_p . According to Lemma C.1 (in appendix C), when all angles are small,

$$\begin{aligned} \angle(T_q, \hat{T}_p) &\leq \angle(T_p, T_q) + \angle(T_p, \hat{T}_p) \\ &\leq O(\varepsilon/\rho) \end{aligned} \quad (\text{IV.11})$$

holds, where we get the second inequality by applying Lemma A.3 (in appendix A). Thus we have:

$$\cos \angle(T_q, \hat{T}_p) = \sqrt{1 - \sin^2 \angle(T_q, \hat{T}_p)} \quad (\text{IV.12})$$

$$\geq \sqrt{1 - (\angle(T_q, \hat{T}_p))^2} \quad (\text{IV.13})$$

$$\geq 1 - (\angle(T_q, \hat{T}_p))^2 \quad (\text{IV.14})$$

$$1 - \cos \angle(T_q, \hat{T}_p) = O(\varepsilon^2/\rho^2). \quad (\text{IV.15})$$

When δ , ε and $r/\rho = 10\varepsilon/\rho$ are small enough, the projection from the local patch $\mathcal{M} \cap B(p, \delta)$ to \hat{T}_p , denoted as $\hat{\Pi}$, is bijective. Denote $\gamma = \angle(T_q, \hat{T}_p)$, then we have

$$\text{vol}(Vr_{\mathcal{M}}(p)) = \int_{\hat{\Pi}(Vr_{\mathcal{M}}(p))} \frac{1}{\cos \gamma} ds \quad (\text{IV.16})$$

$$\leq \max\left(\frac{1}{\cos \gamma}\right) \int_{\hat{\Pi}(Vr_{\mathcal{M}}(p))} ds \quad (\text{IV.17})$$

$$= \max\left(\frac{1}{\cos \gamma}\right) \text{vol}(\hat{\Pi}(Vr_{\mathcal{M}}(p))). \quad (\text{IV.18})$$

Thus by combining (IV.18) with (IV.15), we can have

$$1 \leq \left\| \frac{\text{vol}(Vr_{\mathcal{M}}(p))}{\text{vol}(\hat{\Pi}(Vr_{\mathcal{M}}(p)))} \right\| \leq \frac{1}{\min(\cos \gamma)} = 1 + O(\varepsilon^2/\rho^2). \quad (\text{IV.19})$$

Theorem 4.6 (Voronoi Cell Approximation): Consider the Voronoi cell of point p on the manifold $Vr_{\mathcal{M}}(p)$, and the Voronoi cell on its estimated tangent plane $Vr_{\hat{T}_p}(p)$ built with our algorithm,

$$\left\| \frac{\text{vol}(Vr_{\mathcal{M}}(p))}{\text{vol}(Vr_{\hat{T}_p}(p))} - 1 \right\| \leq O(\varepsilon^2/\rho^2) \quad (\text{IV.20})$$

holds when ε is small enough.

Proof:

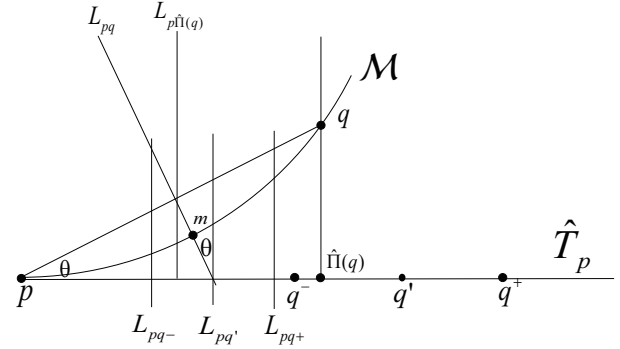


Fig. 4. Parallel bisecting planes.

As described in section III-B, we chose the neighboring points $P_\delta = P \cap B(p, \delta)$, $\delta \geq 10\varepsilon$ for projection. According to Lemma 4.4, for $Vr_{\hat{T}_p}(p)$, any influencing projected point $q \in P_\delta$ satisfies $\|\hat{\Pi}(q) - p\| \leq 2\varepsilon$. Consider $\forall q \in P_\delta$, according to Lemma A.2, A.3 and C.2, we have $\angle(pq, \hat{T}_p) \leq \angle(pq, T_p) + \angle(\hat{T}_p, T_p) = O(\frac{\|p-q\|}{\rho}) + O(r/\rho)$ and $\frac{\|p-q\|}{\|p-\hat{\Pi}(q)\|} - 1 = O(\frac{\varepsilon}{\rho}) + O(\frac{\|p-q\|}{\rho})$. When ε is small enough, we have $(\hat{T}_p \cap B(p, 2\varepsilon)) \subseteq \hat{\Pi}(\mathcal{M} \cap B(p, r))$. Thus we know for $\forall q \in P_\delta$ that satisfies $\|p - \hat{\Pi}(q)\| \leq 2\varepsilon$, $\|p - q\| \leq r = 10\varepsilon$ holds. That is, all neighboring points that could influence $Vr_{\hat{T}_p}(p)$ are included in $P_r = P \cap B(p, r)$. According to Lemma 4.2, we know that all points which may influence $Vr_{\mathcal{M}}(p)$ are also included in P_r .

On the estimated tangent plane \hat{T}_p , we are building 4 sets of Voronoi diagrams to get the converging approximation of the Voronoi cell area, as shown in Figure 4.

For each point $q \in P_\delta$, we consider the bisecting plane L_{pq} between points p and q . We also build the bisecting plane $L_{p\hat{\Pi}(q)}$ for the point-pair $\{p, \hat{\Pi}(q)\}$. As shown in Figure 4, it's obvious that $L_{p\hat{\Pi}(q)} \perp \hat{T}_p$, and the straight line $l_{p\hat{\Pi}(q)} = L_{p\hat{\Pi}(q)} \cap \hat{T}_p$ is also the bisecting line on \hat{T}_p for the point-pair $\{p, \hat{\Pi}(q)\}$. $\{l_{p\hat{\Pi}(q)}\}$ are also the lines that compose $\partial Vr_{\hat{T}_p}(p)$, which is the boundary of the Voronoi cell of p on \hat{T}_p . Notice that for some points $q \in P_\delta$, $l_{p\hat{\Pi}(q)} \cap \partial Vr_{\hat{T}_p}(p) = \emptyset$. That

is, it is not necessary that all bisecting lines contribute to the boundary of $Vr_{\hat{T}_p}(p)$.

Consider the lines $l_{pq} = L_{pq} \cap \hat{T}_p$. Since we have $q\hat{\Pi}(q) \perp \hat{T}_p$ and $pq \perp L_{pq}$, we know that $l_{pq} \perp pq$ and $l_{pq} \perp q\hat{\Pi}(q)$. Thus $l_{pq} \perp p\hat{\Pi}(q)$. Because $L_{p\hat{\Pi}(q)} \perp p\hat{\Pi}(q)$, we know that $l_{pq} \parallel L_{p\hat{\Pi}(q)}$. Then for each l_{pq} , we can build the plane $L_{pq'}$ satisfying $l_{pq} \subset L_{pq'}$ and $L_{pq'} \parallel L_{p\hat{\Pi}(q)}$.

As shown in Figure 4, we denote $\theta = \angle(L_{p\hat{\Pi}(q)}, L_{pq})$. According to Lemma C.2 (in appendix C), we have

$$\theta = \angle(L_{p\hat{\Pi}(q)}, L_{pq}) \quad (\text{IV.21})$$

$$= \angle(p\hat{\Pi}(q), pq) \quad (\text{IV.22})$$

$$\leq \angle(pq, T_p) + \angle(T_p, \hat{T}_p). \quad (\text{IV.23})$$

According to lemma A.2 (in appendix A), we have

$$\sin \angle(pq, T_p) \leq O\left(\frac{\varepsilon}{\rho}\right). \quad (\text{IV.24})$$

According to lemma A.3 (in appendix A), we have

$$\angle(T_p, \hat{T}_p) \leq O\left(\frac{r}{\rho}\right). \quad (\text{IV.25})$$

By combining (IV.24), (IV.25) with (IV.23), we have

$$\sin \theta \leq O\left(\frac{r}{\rho}\right) + O\left(\frac{\varepsilon}{\rho}\right), \quad (\text{IV.26})$$

$$\tan \theta = \frac{\sin \theta}{\cos \theta} \quad (\text{IV.27})$$

$$\leq O\left(\frac{(\varepsilon+r)/\rho}{\sqrt{1 - (\varepsilon+r)^2/\rho^2}}\right) \quad (\text{IV.28})$$

$$\leq O\left(\frac{\varepsilon+r}{\sqrt{\rho^2 - (\varepsilon+r)^2}}\right) \quad (\text{IV.29})$$

$$\leq O\left(\frac{\varepsilon+r}{\rho - \varepsilon - r}\right). \quad (\text{IV.30})$$

We consider the points on the Voronoi cell boundaries: $m \in \partial Vr_{\mathcal{M}}(p)$, as shown in Figure 4. According to Lemma A.2, we have $\sin(\angle(pm, T_p)) \leq O(\varepsilon/\rho)$, since $\|p - m\| \leq \varepsilon$ from Lemma 4.1. When all angles are small, we have

$$\sin(\angle(pm, \hat{T}_p)) \quad (\text{IV.31})$$

$$\leq \sin(\angle(pm, T_p) + \angle(T_p, \hat{T}_p)) \quad (\text{IV.32})$$

$$\leq \sin(\angle(pm, T_p)) + \sin(\angle(T_p, \hat{T}_p)) \quad (\text{IV.33})$$

$$\leq \sin(\angle(pm, T_p)) + \angle(T_p, \hat{T}_p) \quad (\text{IV.34})$$

$$\leq \frac{\varepsilon}{2\rho} + \frac{r}{\rho} \quad (\text{IV.35})$$

$$\leq O\left(\frac{\varepsilon}{\rho}\right) \quad (\text{IV.36})$$

holds since we have $r = 10\varepsilon$. Then we have the bound of the distance from m to \hat{T}_p :

$$d(m, \hat{T}_p) \leq \varepsilon \cdot \sin(\angle(pm, \hat{T}_p)) \leq O(\varepsilon^2/\rho). \quad (\text{IV.37})$$

Suppose $q \in P_\delta$ is the influencing point for $m \in \partial Vr_{\mathcal{M}}(p)$, i.e., $\|p - m\| = \|q - m\|$. By combining (IV.30) with (IV.37),

we have the bound of the distance from m to the plane $L_{pq'}$:

$$d(m, L_{pq'}) = \tan \theta \cdot d(m, \hat{T}_p) \quad (\text{IV.38})$$

$$\leq O\left(\frac{\varepsilon+r}{\rho - \varepsilon - r}\right) \cdot O\left(\frac{\varepsilon^2}{\rho}\right) \quad (\text{IV.39})$$

$$\leq O\left(\frac{\varepsilon^2(\varepsilon+r)}{\rho(\rho - \varepsilon - r)}\right). \quad (\text{IV.40})$$

That is, $\exists c \in \mathbb{R}, c > 0, d(m, L_{pq'}) \leq c \cdot \frac{\varepsilon^2(\varepsilon+r)}{\rho(\rho - \varepsilon - r)}$.

Next we build 2 planes for each $q \in P_\delta$: L_{pq+} and L_{pq-} that satisfy $L_{pq+} \parallel L_{p\hat{\Pi}(q)} \parallel L_{pq-}$, and

$$d(L_{pq+}, L_{pq'}) = d(L_{pq-}, L_{pq'}) \quad (\text{IV.41})$$

$$= c \cdot \frac{\varepsilon^2(\varepsilon+r)}{\rho(\rho - \varepsilon - r)}, \quad (\text{IV.42})$$

$$d(p, L_{pq-}) \leq d(p, L_{pq'}) \leq d(p, L_{pq+}). \quad (\text{IV.43})$$

Since $L_{p\hat{\Pi}(q)} \perp \hat{T}_p$, we know that $L_{pq+} \perp \hat{T}_p, L_{pq-} \perp \hat{T}_p$. As shown in Figure 4, we also have

$$d(p, L_{pq'}) = \frac{\|p - q\|}{2 \cos \theta} \quad (\text{IV.44})$$

As shown in Figure 4, we build the points q', q^+, q^- according to $L_{pq'}, L_{pq+}$ and L_{pq-} , so that these planes are the bisecting planes between the point-pairs $\{p, q'\}$, $\{p, q^+\}$ and $\{p, q^-\}$, respectively.

It's obvious that q', q^+, q^- reside on the same line of $p\hat{\Pi}(q)$. Then we can build the Voronoi diagrams over \hat{T}_p with points $\{p\} \cup \{q^+\}$, $\{p\} \cup \{q'\}$ and $\{p\} \cup \{q^-\}$. Denote the Voronoi cell of p of these diagrams as $Vr^+(p)$, $Vr'(p)$ and $Vr^-(p)$. According to Lemma 4.2 and Lemma 4.4, we can ignore other points $q \notin P_\delta$ without affecting these Voronoi cells for p . Thus we will only use points $q \in P_\delta$.

Since the point cloud P is an $(\varepsilon, s\varepsilon)$ -sample of \mathcal{M} , we have $s\varepsilon \leq \|p - q\| \leq 10\varepsilon$. When ε is small enough, we always have $c \cdot \frac{\varepsilon^2(\varepsilon+r)}{\rho(\rho - \varepsilon - r)} < O(\varepsilon) \leq \frac{\|p - q\|}{2 \cos \theta}$. Thus p will not stay in between L_{pq-} and L_{pq+} . Then we can have:

$$\|p - \hat{\Pi}(q)\| = \|p - q\| \cdot \cos \theta, \quad (\text{IV.45})$$

$$\|p - q'\| = 2 \cdot d(p, L_{pq'}) = \|p - q\| / \cos \theta, \quad (\text{IV.46})$$

$$\|p - q^+\| = \|p - q\| / \cos \theta + 2 \cdot c \cdot \frac{\varepsilon^2(\varepsilon+r)}{\rho(\rho - \varepsilon - r)}, \quad (\text{IV.47})$$

$$\|p - q^-\| = \|p - q\| / \cos \theta - 2 \cdot c \cdot \frac{\varepsilon^2(\varepsilon+r)}{\rho(\rho - \varepsilon - r)}. \quad (\text{IV.48})$$

For $\forall m \in \partial Vr_{\mathcal{M}}(p) \cap L_{pq}$ and its corresponding influencing point q , we have

$$d(m, L_{pq'}) \leq d(L_{pq-}, L_{pq'}), \quad (\text{IV.49})$$

$$d(m, L_{pq'}) \leq d(L_{pq+}, L_{pq'}), \quad (\text{IV.50})$$

$$\|m - p\| = \|m - q\|. \quad (\text{IV.51})$$

So we know that m stays in between L_{pq-} and L_{pq+} of point q . This can lead to:

$$\|m - p\| \leq \|m - q^+\|, \quad (\text{IV.52})$$

$$\|m - p\| \geq \|m - q^-\|. \quad (\text{IV.53})$$

Recall that here q is the influencing point of $m \in \partial Vr_{\mathcal{M}}(p)$. Since $\hat{\Pi}$ is bijective projection, it is obvious

that $\hat{\Pi}(\partial Vr_{\mathcal{M}}(p)) = \partial \hat{\Pi}(Vr_{\mathcal{M}}(p))$. So we have $\forall \hat{m} \in \partial \hat{\Pi}(Vr_{\mathcal{M}}(p))$, $\exists q \in P_\delta$, such that $\|\hat{m} - p\| \geq \|\hat{m} - q\|$. This means that $\partial \hat{\Pi}(Vr_{\mathcal{M}}(p)) \cap (Vr^-(p) - \partial Vr^-(p)) = \emptyset$.

$$\begin{aligned} & \therefore p \in Vr^-(p), p \in \hat{\Pi}(Vr_{\mathcal{M}}(p)), \\ & \therefore Vr^-(p) \subseteq \hat{\Pi}(Vr_{\mathcal{M}}(p)). \end{aligned} \quad (\text{IV.54})$$

Let us assume that $\hat{\Pi}(Vr_{\mathcal{M}}(p)) \subseteq Vr^+(p)$ does not hold, then $\exists m \in (Vr_{\mathcal{M}}(p))$, such that $\|\hat{\Pi}(m) - p\| > \|\hat{\Pi}(m) - q^+\|$ for some $q \in P_\delta$. As shown in Figure 4, m resides in the p -side of plane L_{pq} . Since m also resides on the q^+ -side of plane L_{pq^+} , we have $\min d(m, \hat{T}_p) > d(L_{pq}, L_{pq^+}) \cdot \cot \theta$. Recall that we construct L_{pq^+} so that $d(L_{pq}, L_{pq^+}) \geq \max d(m', \hat{T}_p) \cdot \tan \theta$ for $\forall m' \in Vr_{\mathcal{M}}(p)$. Thus we have $\min d(m, \hat{T}_p) > \max d(m', \hat{T}_p)$ for $\forall m' \in Vr_{\mathcal{M}}(p)$. Thus we have $m \notin Vr_{\mathcal{M}}(p)$, which is contradictory to the assumption. So we have $\hat{\Pi}(Vr_{\mathcal{M}}(p)) \subseteq Vr^+(p)$ holds.

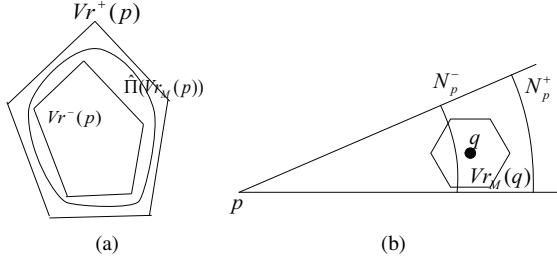


Fig. 5. (a) The nesting of $Vr^-(p)$, $Vr^+(p)$, and $\hat{\Pi}(Vr_{\mathcal{M}}(p))$. (b) The nesting of N_p^- , N_p^+ , and N_{Vp} .

As shown in Figure 5(a), we have

$$Vr^-(p) \subseteq \hat{\Pi}(Vr_{\mathcal{M}}(p)) \subseteq Vr^+(p), \quad (\text{IV.55})$$

which means that:

$$\text{vol}(Vr^-(p)) \leq \text{vol}(\hat{\Pi}(Vr_{\mathcal{M}}(p))) \leq \text{vol}(Vr^+(p)). \quad (\text{IV.56})$$

Since we have $s\varepsilon \leq \|p - q\| \leq r = 10\varepsilon$, by combining equations (IV.45), (IV.46), (IV.47), and (IV.48), we can have

$$\frac{\|p - q^+\|}{\|p - q'\|} \leq 1 + O(\varepsilon^2/\rho^2), \quad (\text{IV.57})$$

$$\frac{\|p - q^-\|}{\|p - q'\|} \geq 1 - O(\varepsilon^2/\rho^2), \quad (\text{IV.58})$$

$$\frac{\|p - q'\|}{\|p - \hat{\Pi}(q)\|} = \frac{1}{\cos^2 \theta} \leq 1 + O(\varepsilon^2/\rho^2). \quad (\text{IV.59})$$

We get the above last equation from Lemma 4.2 and similar calculation as in equation (IV.15) and (IV.36). According to Lemma B.3 (in appendix B), we have

$$\left\| \frac{\text{vol}(Vr^+(p))}{\text{vol}(Vr^+(p))} - 1 \right\| \leq O(\varepsilon^2/\rho^2), \quad (\text{IV.60})$$

$$\left\| \frac{\text{vol}(Vr^-(p))}{\text{vol}(Vr^-(p))} - 1 \right\| \leq O(\varepsilon^2/\rho^2), \quad (\text{IV.61})$$

$$\left\| \frac{\text{vol}(Vr^+(p))}{\text{vol}(Vr_{\hat{T}}(p))} - 1 \right\| \leq O(\varepsilon^2/\rho^2). \quad (\text{IV.62})$$

Finally we have

$$\left\| \frac{\text{vol}(\hat{\Pi}(Vr_{\mathcal{M}}(p)))}{\text{vol}(Vr_{\hat{T}}(p))} - 1 \right\| \leq O(\varepsilon^2/\rho^2). \quad (\text{IV.63})$$

By combining equation (IV.63) with Lemma 4.5, we have

$$\left\| \frac{\text{vol}(Vr_{\mathcal{M}}(p))}{\text{vol}(Vr_{\hat{T}}(p))} - 1 \right\| \leq O(\varepsilon^2/\rho^2). \quad (\text{IV.64})$$

With the convergence of $\text{vol}(Vr_{\hat{T}}(p))$, we are going to prove the convergence of \hat{L}_P^t .

B. Convergence of Integration Approximation

Recall that in our algorithm, the approximation LBO Δ_P^t in equation (III.3) is defined as:

$$\Delta_P^t f(p) = \frac{1}{4\pi t^2} \sum_{q \in P_\delta} (e^{-\frac{\|q-p\|^2}{4t}} (f(q) - f(p)) \text{vol}(Vr_{\hat{T}}(q))),$$

where $Vr_{\hat{T}}(q)$ is the Voronoi cell of the point q over \hat{T}_q . In order to prove that Δ_P^t is converging to the continuous LBO $\Delta_{\mathcal{M}}$, we introduce the following intermediate LBO:

$$\check{\Delta}_P^t f(p) = \frac{1}{4\pi t^2} \sum_{q \in P_\delta} (e^{-\frac{\|q-p\|^2}{4t}} (f(q) - f(p)) \text{vol}(Vr_{\mathcal{M}}(q))). \quad (\text{IV.65})$$

It is obvious that the only difference between Δ_P^t and $\check{\Delta}_P^t$ is that we use $Vr_{\hat{T}}(q)$ instead of $Vr_{\mathcal{M}}(q)$ as in (IV.65), because it is impossible to get $\text{vol}(Vr_{\mathcal{M}}(q))$ in most real applications. In the following Lemma 4.10 we will show that $\check{\Delta}_P^t$ is converging to the continuous LBO $\Delta_{\mathcal{M}}$. And based on the Voronoi cell area convergence result in Theorem 4.6, we will show in Theorem 4.11 that our approximation LBO Δ_P^t is converging to $\check{\Delta}_P^t$, which means that Δ_P^t is converging to $\Delta_{\mathcal{M}}$ as well.

Definition 4.7: For $\forall p \in P$, recall we have $P_\delta = P \cap B(p, \delta)$. Define the following patches of the manifold surface:

$$N_p = \mathcal{M} \cap B(p, \delta) \quad (\text{IV.66})$$

$$N_{Vp} = \cup_{q \in P_\delta} Vr_{\mathcal{M}}(q) \quad (\text{IV.67})$$

$$N_p^+ = \mathcal{M} \cap B(p, 1.1\delta) \quad (\text{IV.68})$$

$$N_p^- = \mathcal{M} \cap B(p, 0.9\delta) \quad (\text{IV.69})$$

given $\delta \geq 10\varepsilon$.

According to Lemma A.5, the continuous LBO $\Delta_{\mathcal{M}}$ can be computed as the integration over the whole manifold \mathcal{M} . Our essential idea is to approximate such integration locally over N_{Vp} instead, because local integration approximation could produce sparse matrix operator instead of dense matrix from global integration approximation and reduce effort of solving related eigen problem greatly. The following Lemma 4.9 shows that such local approximation is reasonable, which can lead to the convergence of $\check{\Delta}_P^t$ to $\Delta_{\mathcal{M}}$, as shown in Lemma 4.10. In order to prove Lemma 4.9, we need to show that N_{Vp} is bounded in between N_p^- and N_p^+ (as shown in Figure 5(b)), independent of the sampling size ε , which is addressed in the following Lemma 4.8.

Lemma 4.8 (Bound of N_{Vp}):

$$N_p^- \subseteq N_{Vp} \subseteq N_p^+. \quad (\text{IV.70})$$

Proof: This nesting relationship is shown in Figure 5(b).

First we prove $N_p^- \subseteq N_{Vp}$: For $\forall m \in N_p^-$, there exists $\exists q \in P$, such that $m \in Vr_{\mathcal{M}}(q)$. According to Lemma 4.1, we have $\|q - m\| \leq \varepsilon$.

$$\because \|p - q\| \leq \|p - m\| + \|q - m\| \leq 0.9\delta + \varepsilon \leq \delta,$$

$$\therefore q \in P_\delta, Vr_{\mathcal{M}}(q) \subseteq N_{Vp}, m \in N_{Vp}.$$

Next we prove $N_{Vp} \subseteq N_p^+$: For $\forall m \in N_{Vp}$, there exists $\exists q \in P_\delta, m \in Vr_{\mathcal{M}}(q)$. Recall that $\|q - m\| \leq \varepsilon$ and $\|p - q\| \leq \delta$, so we have $\|p - m\| \leq \|p - q\| + \|q - m\| \leq \delta + \varepsilon \leq 1.1\delta$. Thus $m \in N_p^+$. ■

Lemma 4.9 (Approximation using N_{Vp}):

$$\int_{N_{Vp}} e^{-\frac{\|p-y\|}{4t}} f(y) d\mu_y - \int_{\mathcal{M}} e^{-\frac{\|p-y\|}{4t}} f(y) d\mu_y = o(t^l), \quad (\text{IV.71})$$

for any positive natural number l .

Proof: Similar to the proof of Lemma A.4, which is Lemma 1 in [24]:

$$\begin{aligned} & \left| \int_{N_{Vp}} e^{-\frac{\|p-y\|}{4t}} f(y) d\mu_y - \int_{\mathcal{M}} e^{-\frac{\|p-y\|}{4t}} f(y) d\mu_y \right| \\ &= \left| \int_{\mathcal{M} - N_{Vp}} e^{-\frac{\|p-y\|}{4t}} f(y) d\mu_y \right| \\ &\leq \text{vol}(\mathcal{M}) \sup_{x \in \mathcal{M}, x \notin N_{Vp}} (|f(x)|) e^{-\frac{d_1^2}{4t}} \end{aligned} \quad (\text{IV.72})$$

$$\leq \text{vol}(\mathcal{M}) \sup_{x \in \mathcal{M}, x \notin N_p^-} (|f(x)|) e^{-\frac{d_2^2}{4t}} = o(t^l), \quad (\text{IV.73})$$

where $d_1 = \inf_{x \notin N_{Vp}} \|p - x\|$, and $d_2 = \inf_{x \notin N_p^-} \|p - x\|$. ■

Lemma 4.10 (Convergence of $\tilde{\Delta}_P^t$ to $\Delta_{\mathcal{M}}$):

$$\lim_{\varepsilon \rightarrow 0} \|\tilde{\Delta}_P^t f - \Delta_{\mathcal{M}} f\|_\infty = 0, \quad (\text{IV.74})$$

where $t(\varepsilon) = \varepsilon^{\frac{1}{2+\xi}}$, and $\xi > 0$ is any positive fixed number.

Proof:

Note that $\varepsilon = t^{2+\xi}$. According to Lemma 4.1, we know $\forall y \in Vr_{\mathcal{M}}(q), \|y - q\| \leq \varepsilon$ or $\|y - q\| \leq O(\varepsilon)$. According to Lemma A.5, we can approximate $\Delta_{\mathcal{M}}$ using integration over

\mathcal{M} . Thus we have:

$$\lim_{t \rightarrow 0} \left| \tilde{\Delta}_P^t f(p) - \int_{N_{Vp}} e^{-\frac{\|p-y\|}{4t}} (f(y) - f(p)) d\mu_y \right| \quad (\text{IV.75})$$

$$= \lim_{t \rightarrow 0} \left| \sum_{q \in P_\delta} \int_{Vr_{\mathcal{M}}(q)} \frac{1}{4\pi t^2} [e^{-\frac{\|q-p\|^2}{4t}} (f(q) - f(p)) - e^{-\frac{\|y-p\|^2}{4t}} (f(y) - f(p))] d\mu_y \right| \quad (\text{IV.76})$$

$$= \lim_{t \rightarrow 0} \left| \sum_{q \in P_\delta} \int_{Vr_{\mathcal{M}}(q)} \frac{1}{4\pi t^2} [e^{-\frac{\|q-p\|^2}{4t}} (f(q) - f(p)) - e^{-\frac{\|q-p\|^2}{4t}} (f(y) - f(p)) + e^{-\frac{\|q-p\|^2}{4t}} (f(y) - f(p)) - e^{-\frac{\|y-p\|^2}{4t}} (f(y) - f(p))] d\mu_y \right| \quad (\text{IV.77})$$

$$= \lim_{t \rightarrow 0} \left| \sum_{q \in P_\delta} \int_{Vr_{\mathcal{M}}(q)} \frac{1}{4\pi t^2} e^{-\frac{\|y-p\|^2}{4t}} [e^{\frac{\|y-p\|^2 - \|q-p\|^2}{4t}} (f(q) - f(y)) + (e^{\frac{\|y-p\|^2 - \|q-p\|^2}{4t}} - 1)(f(y) - f(p))] d\mu_y \right| \quad (\text{IV.78})$$

$$\leq \lim_{t \rightarrow 0} \sum_{q \in P_\delta} \int_{Vr_{\mathcal{M}}(q)} \frac{1}{4\pi t^2} e^{-\frac{\|y-p\|^2}{4t}} [|f(y) - f(p)| \cdot |e^{-\frac{O(\varepsilon)}{4t}} - 1| + |e^{-\frac{O(\varepsilon)}{4t}} O(\varepsilon)|] d\mu_y \quad (\text{IV.79})$$

$$\leq \lim_{t \rightarrow 0} \frac{(\|f\|_\infty - f(p)) \cdot |e^{-\frac{O(\varepsilon)}{4t}} - 1| + O(\varepsilon)}{t} \int_{N_{Vp}} \frac{1}{4\pi t} e^{-\frac{\|y-p\|^2}{4t}} d\mu_y \quad (\text{IV.80})$$

$$\leq \lim_{t \rightarrow 0} \frac{(\|f\|_\infty - f(p)) |e^{-\frac{O(\varepsilon)}{4t}} - 1| + O(\varepsilon)}{t} \quad (\text{IV.81})$$

$$\leq \lim_{t \rightarrow 0} \frac{O(\varepsilon/t) + O(\varepsilon)}{t} \quad (\text{IV.82})$$

$$= \lim_{t \rightarrow 0} \frac{O(t^{1+\xi}) + O(t^{2+\xi})}{t} = 0 \quad (\text{IV.83})$$

In the above derivation, we applied $\|q - p\| - \|y - q\| \leq \|y - p\| \leq \|q - p\| + \|y - q\|$, $\|y - q\| \leq \varepsilon$, $|f(y) - f(q)| = O(\|y - q\|)$ (since $f \in C^2$) and $\|y - q\| \leq \varepsilon$ on equation (IV.78) to get equation (IV.79). By applying the following inequality to equation (IV.80), we get equation (IV.81).

$$\int_{N_{Vp}} \frac{1}{4\pi t} e^{-\frac{\|y-p\|^2}{4t}} d\mu_y \quad (\text{IV.84})$$

$$= \int_{\hat{\Pi}(N_{Vp})} \frac{1}{4\pi t} e^{-\frac{\|\hat{\Phi}(y)-p\|^2}{4t}} |J(\hat{\Phi})|_y d\mu_y \quad (\text{IV.85})$$

$$\leq \int_{\hat{\Pi}(N_{Vp})} \frac{1}{4\pi t} e^{-\frac{\|y-p\|^2}{4t}} |J(\hat{\Phi})|_y d\mu_y \quad (\text{IV.86})$$

$$\leq \max_{y \in \hat{\Pi}(N_p^+)} (|J(\hat{\Phi})|_y) \int_{\hat{\Pi}_p} \frac{1}{4\pi t} e^{-\frac{\|y-p\|^2}{4t}} d\mu_y \quad (\text{IV.87})$$

$$\leq \max_{y \in \hat{\Pi}(N_p^+)} (|J(\hat{\Phi})|_y) = \text{Constant}. \quad (\text{IV.88})$$

Here J stands for the Jacobian Matrix.

By combining Lemma A.5 and Lemma 4.9 with equation (IV.83), we have $\lim_{\varepsilon \rightarrow 0} \|\tilde{\Delta}_P^t f - \Delta_{\mathcal{M}} f\|_\infty = 0$ proved. ■

Theorem 4.11 (Convergence of Δ_P^t to $\Delta_{\mathcal{M}}$): Consider an $(\varepsilon, s\varepsilon)$ -sample P of the closed manifold surface \mathcal{M} , and an arbitrary function $f \in C^2$, our discrete LBO operator Δ_P^t satisfies:

$$\lim_{\varepsilon \rightarrow 0} \|\Delta_P^t f - \Delta_{\mathcal{M}} f\|_{\infty} = 0, \quad (\text{IV.89})$$

where $t(\varepsilon) = \varepsilon^{\frac{1}{2+\xi}}$, and $\xi > 0$ is any positive fixed number.

Proof:

According to Theorem 4.6, we have

$$\left\| \frac{\text{vol}(Vr_{\mathcal{M}}(p))}{\text{vol}(Vr_{\hat{T}}(p))} - 1 \right\| = O\left(\frac{\varepsilon^2}{\rho^2}\right). \quad (\text{IV.90})$$

Thus:

$$\left\| \frac{\hat{\Delta}_P^t f(p)}{\Delta_P^t f(p)} - 1 \right\| = O\left(\frac{\varepsilon^2}{\rho^2}\right), \quad (\text{IV.91})$$

which means:

$$\lim_{t \rightarrow 0} \|\hat{\Delta}_P^t f(p) - \Delta_P^t f(p)\|_{\infty} = 0. \quad (\text{IV.92})$$

By combining (IV.92) with Lemma 4.10, we have this theorem proved. ■

V. EXPERIMENTAL RESULTS

Experiments are conducted to verify the convergence property of our operator \hat{L}_P^t proved in section IV, the convergence property of the eigen-vectors $\{H^i\}$, the geometry-awareness of $\{H^i\}$ and applications of PB-MHT for spectral geometry processing. In our implementation, the generation of the LBO matrix is developed using MinGW, the eigen problem is solved in MATLAB, and the filtering and rendering parts are written in Visual C++. We conduct experiments on a Windows XP platform with Intel Core 2 Duo 2.66GHz CPU and 2GB DDR2 RAM. Table I shows the model information and the running time of our experiments.

TABLE I
MODEL INFORMATION AND RUNNING TIME (IN SECONDS) FOR COMPUTING THE LBO MATRIX (t_{LBO}) AND SOLVING THE EIGEN-VECTORS (t_{eigen}).

Model	#Points	t_{LBO}	#Bases	t_{eigen}
Sphere	4,002	156	100	2.8
Eight	7,678	401	100	17
Cylinder	90,300	6,426	100	348
Rabbit	248,304	12,198	100	2,051
Chinese Lion	611,222	25,214	100	7,269

A. Operator Convergence

To verify the convergence of our LBO matrix \hat{L}_P^t , we use a cylinder model with radius 1, height 4, and 90,300 vertices. We parameterize this cylinder surface as:

$$x = \cos \alpha, \quad (\text{V.1})$$

$$y = \sin \alpha, \quad (\text{V.2})$$

$$z = v, \quad (\text{V.3})$$

where α and v are the parameters: $0 \leq \alpha < 2\pi$, $0 < v < 4$. We sample the cylinder circle with 300 points, and sample the

v direction with 301 points. We define the function f over the cylinder surface as:

$$f(p) = v^2. \quad (\text{V.4})$$

The analytical solution of the continuous LBO applied on the function f is $\Delta_{\mathcal{M}} f = 2$, for $v > 0$ over this cylinder surface. In this paper we only consider closed surfaces, but it is impractical to conduct experiments on infinite-length cylinder surfaces. So in our experiments we use the cylinder model of finite length and ignore the solutions for points near the boundary to verify the performance of operators on the infinite cylinder surface. We give each point an index according to its v parameter value. Figure 6 shows the approximation results of our LBO applied on the function (a) $\hat{L}_P^t \mathbf{f}$, as compared to (b) Belkin *et al*'s LBO [1] $L_P^t \mathbf{f}$, (c) the graph Laplacian $L_G \mathbf{f}$, and (d) the trivial extension of $1/2 \cdot (L_P^t + (L_P^t)^T) \mathbf{f}$. If we ignore the cylinder boundary points, which indices are close to 0 and 9×10^4 as in Figure 6, we can see that: (a) our \hat{L}_P^t is converging perfectly; (b) Belkin *et al*'s L_P^t has slight oscillations; (c) the graph Laplacian L_G gives constant 0 values incorrectly; and (d) the trivial extension $(L_P^t + (L_P^t)^T)/2$ does not converge at all.

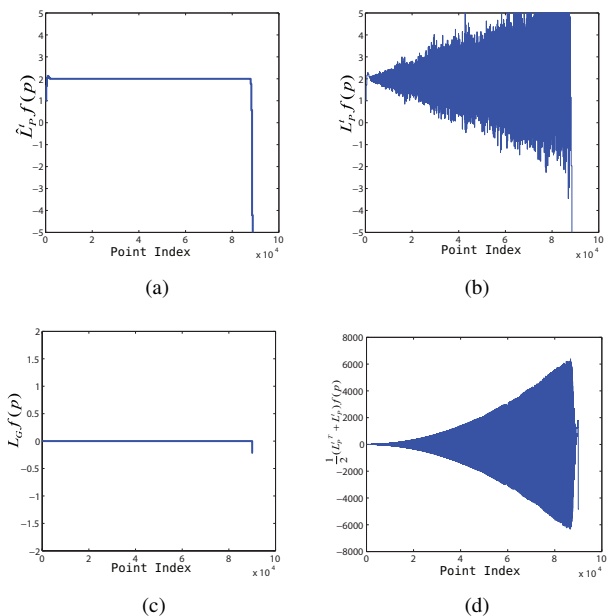


Fig. 6. LBO approximation result on the cylinder surface: (a) our Voronoi cell-based operator \hat{L}_P^t ; (b) Belkin *et al*'s operator L_P^t ; (c) the graph Laplacian operator L_G ; (d) the trivial extension $(L_P^t + (L_P^t)^T)/2$. Note that (d) has much larger scale than others.

The reason why Belkin *et al*'s LBO L_P^t has more error, as shown in Figure 1(a), is that L_P^t is actually trying to compute the integration on estimated tangent plane rather than the integration over the manifold as proposed by Lemma A.5. Although this is still converging, there may be more error. In Figure 6, the point index depends on v parameter, that is, the higher the index, the higher function value will the point and its neighbours have, since $f(p) = v^2$. This may “amplify” the error as the index gets larger. Our LBO \hat{L}_P^t , as shown in Figure 1(b), approximates the integration over the manifold directly with the estimated Voronoi cell area.

The LBO on the 2-sphere in \mathbb{R}^3 is well studied. Eigenfunctions of the LBO over the sphere are called Spherical Harmonics and denoted as Y_l^m with degree l and order m . In spherical coordinates, the eigen-function of LBO with the smallest eigen-value $\lambda = 2$ on the unit sphere is $Y_1^0 = \cos \theta$. That is, $\Delta_{S(2)} Y_1^0 = -2Y_1^0$. We use three point clouds sampled from the 2-sphere of unit radius: uniform 1,000 points, uniform 3,994 points, and 2,475 points with different resolutions on its two hemispheres, as shown in Figure 7. For each point, we compute the error between the approximated $\Delta_{S(2)} Y_1^0$ and the analytical result $-2Y_1^0$. Figure 8 shows the error histograms of \hat{L}_P^t and L_P^t on these sphere models with input function $f = Y_1^0$. In all cases \hat{L}_P^t has less error than L_P^t .

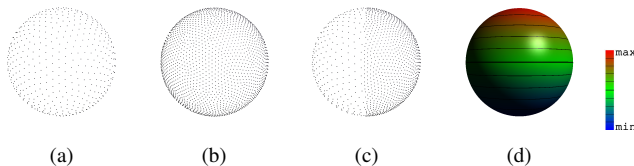


Fig. 7. Different point clouds sampled on unit sphere: (a) uniform 1,000 points; (b) uniform 3,994 points; (c) non-uniform 2,475 points; (d) Spherical Harmonics Y_1^0 on unit sphere.

B. Eigen-Vector Convergence

We use the same sphere models as in section V-A. Note that because sphere is rotational symmetric, Y_l^m can be rotated over surface for any angle. In spherical coordinates, we have $Y_1^0 = \cos \theta$. In the spectrum of the unit 2-sphere in \mathbb{R}^3 , Y_1^0 has multiplicity of 3 with $\lambda = 2$. In other words, Y_1^0 appears 3 times with different rotation. Table II shows the error of the first 3 eigen-vectors with the non-zero eigen-values of \hat{L}_P^t . We can see they are very close to the analytical result Y_1^0 and 2, respectively.

TABLE II
ERROR OF \hat{L}_P^t EIGEN-VECTORS ON UNIT SPHERE

Y_l^m	Range of H	#Points	H	$\ H - Y\ _{\text{inf}}$	λ
Y_1^0	[-0.5, 0.5]	1,000	H^1	0.0009	1.9882
			H^2	0.0008	1.9890
			H^3	0.0007	1.9903
		Non-Uniform	H^1	0.0041	1.9779
			H^2	0.0015	1.9913
			H^3	0.002	1.9917
		2,475	H^1	0.0008	1.9952
			H^2	0.00025	1.9953
			H^3	0.0006	1.9957

We also compute the error data for the linear FEM-based discrete LBO eigen-vectors [4], to compare with our results. Note that the FEM-based discrete LBO depends on mesh connectivity, thus can not be applied to point clouds directly. We use a triangulated mesh with the exact set of vertices as the point clouds. As shown in table III, the FEM-based discrete LBO does provide eigen-vectors close to the analytical counterparts (less accurate than our LBO though), but it yields an eigen-value close to 8 rather than the analytical result of 2.

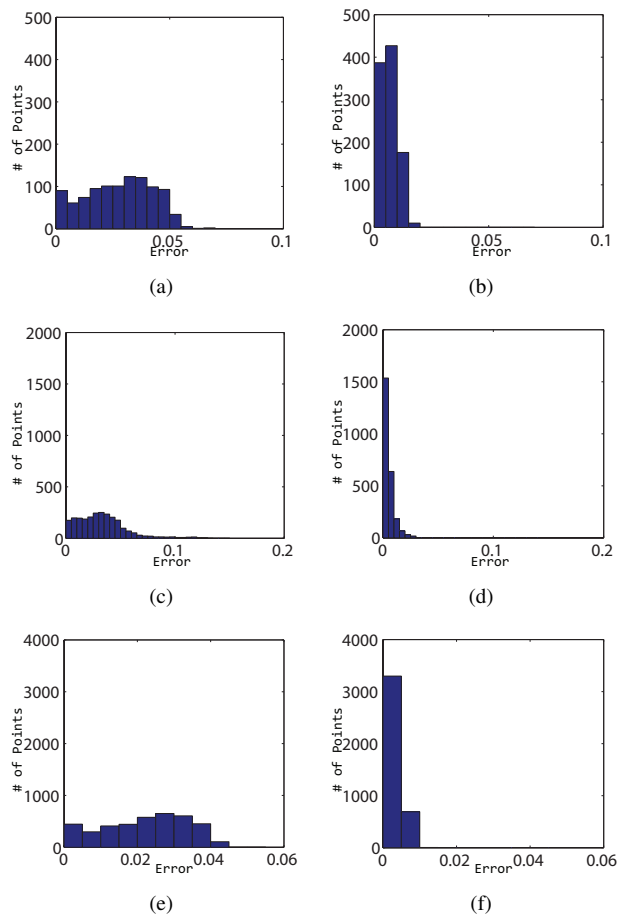


Fig. 8. Approximation result of $\Delta_{S(2)} Y_1^0$ on the unit sphere. Left column is the error histogram of Belkin *et al*'s operator L_P^t ; right column is the error histogram of our new operator \hat{L}_P^t : (a), (b) uniformly sampled 1,000 points; (c), (d) non-uniformly sampled 2,475 points; (e), (f) uniformly sampled 3,994 points.

TABLE III
ERROR OF FEM-BASED LAPLACIAN EIGEN-VECTORS ON UNIT SPHERE

Y_l^m	Range of H	#Points	H	$\ H - Y\ _{\text{inf}}$	λ
Y_1^0	[-0.5, 0.5]	1,000	H^1	0.0103	7.999
			H^2	0.0095	8.0002
			H^3	0.0087	8.0004
		Non-Uniform	H^1	0.0118	7.9994
			H^2	0.0085	7.9998
			H^3	0.0102	8.0005
		2,475	H^1	0.0048	7.9998
			H^2	0.0069	8.0001
			H^3	0.0019	8.0001

Figure 9 shows the first three eigen-vectors of the graph Laplacian L_G , which are not close to the analytical counterpart as shown in Figure 7(d).

C. Non-Uniformly-Sampled Point Cloud

Our experiments show that as long as the point cloud P is $(\varepsilon, s\varepsilon)$ -sampled, and the local feature sizes ρ are not close to zero (since our LBO convergence rate is $O(\frac{\varepsilon^2}{\rho^2})$), our PB-MHB is geometry-aware and independent of the sampling rate. We conduct our experiment on the ‘‘symmetric’’ two-hole torus (‘‘Eight’’) model, where the point sampling rate over the two

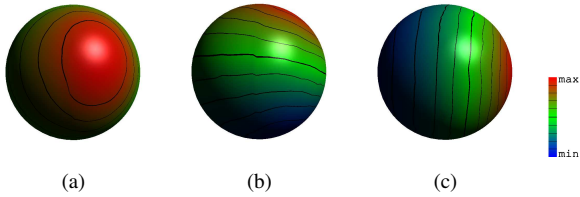


Fig. 9. Eigen-vectors of graph Laplacian L_G on the non-uniform sphere model as in Figure 7(c): (a) H^1 ; (b) H^2 ; (c) H^3 .

handles are different. As shown in Figure 10, when the point distribution is non-uniform, the first 4 bases of our PB-MHB are still symmetric over the surface, while the eigen-vectors of the graph Laplacian operator can not follow the geometry property of the surface.

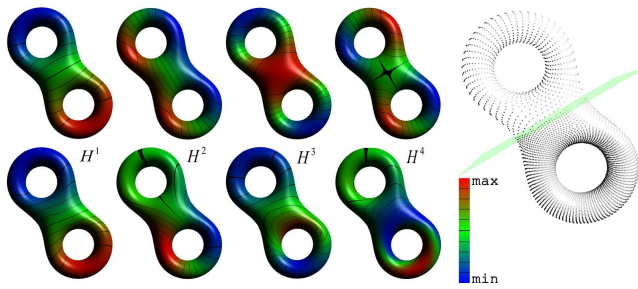


Fig. 10. The eigen-functions H^1 , H^2 , H^3 , and H^4 of our \hat{L}_P^t (first row) and the graph Laplacian operator L_G (second row), for the symmetric model “Eight” with non-uniform sampling rate.

D. Spectral Filtering

Spectral filtering could be used for model manipulation such as noise-removing. Having the PB-MHB, we can apply filtering on the spectral representation of point-sampled surfaces. As shown in Figure 2, we can apply either “low-pass filtering” or “detail-enhancement” on the point-sampled Chinese Lion model. Note that even when points are non-uniformly distributed, as shown in Figure 11 where the left-part of the Rabbit model is sparser than the right-part, our PB-MHT can still get “symmetric” filtering result, while the graph Laplacian method makes the left-part “shrink” more than the right-part. Figure 12 shows the example of removing the high-frequency noises on the sphere by applying the low-pass filter with PB-MHT, which still preserves the symmetry of the sphere.

VI. CONCLUSION AND FUTURE WORK

The mesh-based Manifold Harmonics [4], [5] provides spectral processing framework for 3D models. However, it can not be applied to point clouds directly. In this paper, we propose a new method to compute the *symmetric* and *converging* discrete LBO matrix \hat{L}_P^t on the manifold surface \mathcal{M} represented by the point cloud P . We prove that \hat{L}_P^t is converging point-wisely to the continuous LBO $\Delta_{\mathcal{M}}$ given that P is $(\varepsilon, s\varepsilon)$ -sampled, and the local feature sizes at the points are not close to zero. With the symmetric property of \hat{L}_P^t , we can compute the Point-Based Manifold Harmonic

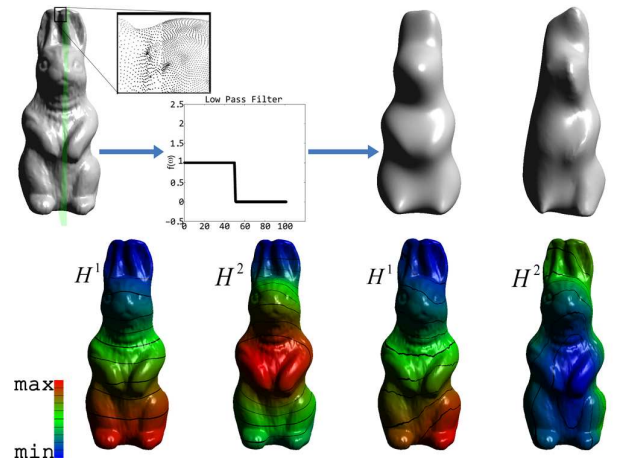


Fig. 11. First row: the Rabbit model with non-uniform sampling, and the low-pass filtered model: using our \hat{L}_P^t (left) and graph Laplacian operator L_G (right). Second row: H^1 and H^2 of our \hat{L}_P^t (left) and the graph Laplacian operator L_G (right). It’s obvious that \hat{L}_P^t is geometry-aware and L_G is not.

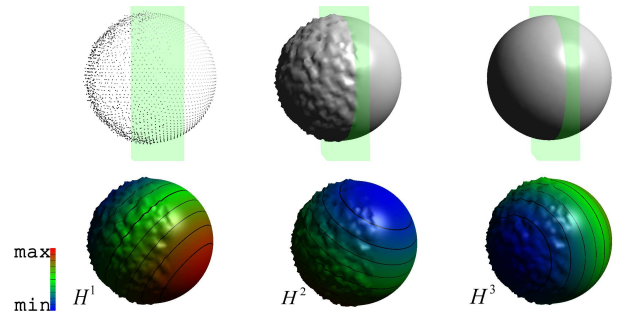


Fig. 12. First row: the sphere model with noises on its left side, before and after the low-pass filtering. Second row: the H^1 , H^2 , and H^3 bases.

Bases $\{H^i\}$ on point clouds by solving the eigen problem $\hat{L}_P^t f = \lambda f$. The orthogonal bases can be used to perform spectral transformation and processing directly on point clouds without computing the explicit global mesh. Our experiments show that \hat{L}_P^t converges very well as compared to both the graph Laplacian operator and the trivial extension of Belkin *et al*’s discrete operator [1]. We also demonstrate that our PB-MHT can be used as an effective spectral analysis and processing tool for point-sampled manifold surfaces.

There are also some limitations about our current approach, which motivates our future researches along this direction of point-based spectral processing. First of all, this method is designed for closed manifold surfaces. When there is boundary on surfaces, it is hard for the algorithm to estimate the tangent plane near the boundary robustly. Thus the performance of this method degrades significantly at the boundary points. We will investigate robust algorithms for open point-sampled surfaces.

Second, our current method is based on the assumption that the point cloud is $(\varepsilon, s\varepsilon)$ -sampled, and the local feature sizes are not close to zero. For the surface regions with high curvature, our current method requires high sampling rates to produce meaningful discrete operator. This method is built based on the assumption that the point set is sampled on the differentiable manifold surface. When there is sharp edges or spikes in the model, the performance will decrease because

the local feature sizes at those sharp edges or spikes tend to be zero. Since our LBO convergence rate is $O(\frac{\varepsilon^2}{\rho^2})$, if the point cloud is not dense enough locally at those regions, this algorithm will have difficulty in converging to the continuous counterpart. Computing the spectral bases for the point-sampled surfaces with sharp features will be an interesting research avenue for the future.

APPENDIX A REFERRED LEMMAS

This section shows the Lemmas that we referred from other papers. These Lemmas are used in our proof of convergence in section IV.

Lemma A.1 (Lemma 3.1 in [25]): Given two points $p, q \in \mathcal{M}$ with $\|p - q\| \leq \rho/3$, the angle between their normals n_p and n_q satisfies $\angle(n_p, n_q) < \frac{\|p-q\|}{\rho - \|p-q\|}$.

Lemma A.2 (Lemma 6 in [32]): For any point $p, q \in \mathcal{M}$ with $\|p - q\| < \rho$, we have that $\sin \angle(pq, T_p) \leq \frac{\|q-p\|}{2\rho}$, and the distance from q to T_p is bounded by $\frac{\|q-p\|^2}{2\rho}$, where ρ is the local feature size of p , T_p is the tangent plane at p .

Lemma A.3 (Theorem 3.2 in [1]): Suppose P is an ε -sample of \mathcal{M} . For $p \in P$ with local feature size ρ and real tangent plane T_p . Compute \hat{T}_p as in Algorithm PCDLaplace [1], $\angle(T_p, \hat{T}_p) = O(r/\rho)$ for $r < \rho/2$ and $r \geq 10\varepsilon$.

Lemma A.4 (Lemma 1 in [24]): Given any openset $B \subset \mathcal{M}$, $p \in B$, for any positive natural number l ,

$$\int_{B \subset \mathcal{M}} e^{-\frac{\|p-y\|}{4t}} f(y) d\mu_y - \int_{\mathcal{M}} e^{-\frac{\|p-y\|}{4t}} f(y) d\mu_y = o(t^l).$$

Lemma A.5 (Lemma 5 in [24]):

$$\Delta_{\mathcal{M}} f(p) = \lim_{t \rightarrow 0} \frac{1}{4\pi t^2} \left(\int_{\mathcal{M}} e^{-\frac{\|p-y\|}{4t}} f(p) d\mu_y - \int_{\mathcal{M}} e^{-\frac{\|p-y\|}{4t}} f(y) d\mu_y \right).$$

APPENDIX B LEMMAS ABOUT VORONOI CELLS

In this paper we are using the Voronoi cells $Vr_{\hat{T}}(p)$ on the estimated tangent planes \hat{T}_p . This appendix section shows some results that are related to Voronoi cells over 2-planes and are used for our convergence proof of Theorem 4.6.

Lemma B.1: For plane L and point set $P \subset L$, consider the Voronoi diagram of P over L . Let $p \in P$. Suppose the Voronoi cell of p is $Vr(p)$ and the cell boundary is $\partial Vr(p)$. $\forall \tilde{p} \in \partial Vr(p)$, $\|p - \tilde{p}\| \leq \varepsilon$.

If we fix point p and move all the other points $q \in P$ as: $q' = p + (q - p) \cdot t$, $t > 0$, Then the area of the new Voronoi cell $Vr'(p)$ has such property:

$$\frac{\text{vol}(Vr'(p))}{\text{vol}(Vr(p))} = t^2. \quad (\text{B.1})$$

Proof:

Suppose the plane L is parameterized in (u, v) coordinates with p being the origin. For point $q_i \in P$ and corresponding displaced point q'_i , we have their coordinate relationship: $(u'_i, v'_i) = t(u_i, v_i)$.

So we can build the mapping $f : L \rightarrow L$ as $m' = f(m) = f(u, v) = (tu, tv)$, where $m, m' \in L$. Thus we have

$$\begin{aligned} \forall m \in L, \|m' - p\| &= t\|m - p\|, \\ \forall m \in L, \|m' - q_i\| &= t\|m - q_i\|. \end{aligned}$$

It's obvious that $m \in Vr(p) \leftrightarrow m' = f(m) \in Vr'(p)$. Then we have

$$\text{vol}(Vr'(p)) = \int_{Vr'(p)} du' dv' = \int_{Vr(p)} t^2 dudv = t^2 \text{vol}(Vr(p)). \quad \blacksquare$$

Lemma B.2: Consider plane L and point set $P \subset L$, as defined in Lemma B.1. If we move one point $q \in P$ as: $q' = p + (q - p) \cdot t$, $0 < t < 1$, then the area of the new Voronoi cell $Vr'(p)$ has such property:

$$\text{vol}(Vr'(p)) \leq \text{vol}(Vr(p)). \quad (\text{B.2})$$

Proof:

Suppose l_{pq} and $l_{pq'}$ are the bisecting planes between the point-pairs $\{p, q\}$ and $\{p, q'\}$. $\forall m \in Vr'(p)$, we have $\|m - p\| < \|m - q'\|$. That is, m resides on the p -side of $l_{pq'}$. As shown in Figure 13, it is obvious that $l_{pq'}$ resides on the p -side of l_{pq} . Thus we have $m \in Vr(p)$.

Thus $Vr'(p) \subseteq Vr(p)$. \blacksquare

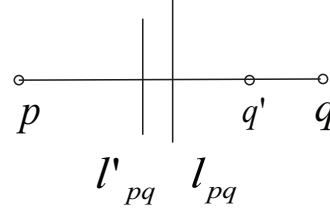


Fig. 13. Moving a point in the Voronoi diagram.

Lemma B.3: Consider plane L and point set $P \subset L$, as defined in Lemma B.1. If we fix point p and move all the other points $q \in P$ as: $q' = p + (q - p) \cdot t_q$, $t_q > 0$, then we have the following result about the new Voronoi cell $Vr'(p)$:

$$(\min(t_q))^2 \leq \frac{\text{vol}(Vr'(p))}{\text{vol}(Vr(p))} \leq (\max(t_q))^2. \quad (\text{B.3})$$

Proof: From Lemma B.2, we know that the area of $Vr'(p)$ will change monotonically with t_q . So combine it with Lemma B.1 we can get this lemma proved. \blacksquare

APPENDIX C LEMMAS ABOUT SMALL ANGLES

This section shows the Lemmas about small angles that we used for the equation (IV.23) in the proof of Theorem 4.6.

Lemma C.1 (Angles of 3 Planes): Consider 3 planes T_1 , T_2 and T_3 with their corresponding unit normal vectors \mathbf{n}_1 , \mathbf{n}_2 and \mathbf{n}_3 . Denote $\angle(\mathbf{n}_1, \mathbf{n}_2) = \alpha$, $\angle(\mathbf{n}_2, \mathbf{n}_3) = \beta$, $\angle(\mathbf{n}_1, \mathbf{n}_3) = \gamma$. Without any loss of generality, assume α, β, γ are all acute angles.

If $\alpha < \pi/4$, $\beta < \pi/4$, then we have $\gamma \leq \alpha + \beta$ holds.

Proof:

Since we are observing 3 unit vectors, it's convenient to put them on unit sphere S , as shown in Figure 14 (left). Consider the geodesic distance $g(\mathbf{n}_1, \mathbf{n}_2)$, $g(\mathbf{n}_2, \mathbf{n}_3)$ and $g(\mathbf{n}_1, \mathbf{n}_3)$ on S . It's obvious that all these geodesics are part of great circles of S . From the definition of geodesic distance, we know that $g(\mathbf{n}_1, \mathbf{n}_3) \leq g(\mathbf{n}_1, \mathbf{n}_2) + g(\mathbf{n}_2, \mathbf{n}_3)$. Since S is unit sphere, we also have $g(\mathbf{n}_1, \mathbf{n}_2) = \alpha$, $g(\mathbf{n}_2, \mathbf{n}_3) = \beta$, $g(\mathbf{n}_1, \mathbf{n}_3) = \gamma$. So we have $\gamma \leq \alpha + \beta$ holds. ■

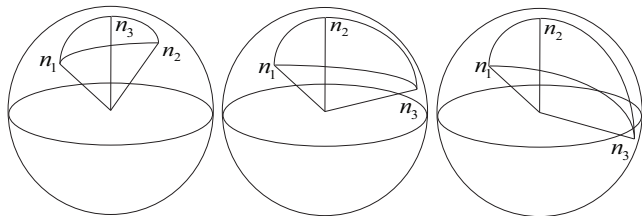


Fig. 14. Unit vectors on the unit sphere: Lemma C.1 (left) and Lemma C.2 (middle and right).

Lemma C.2 (Angles of 2 Planes and 1 Vector): Consider 2 planes T_1 and T_2 with their corresponding unit normal vectors \mathbf{n}_1 and \mathbf{n}_2 . Consider another unit vector \mathbf{n}_3 . Denote $\angle(\mathbf{n}_1, \mathbf{n}_2) = \alpha$, $\angle(T_2, \mathbf{n}_3) = \beta$, $\angle(T_1, \mathbf{n}_3) = \gamma$.

If $\alpha < \pi/4$, $\beta < \pi/4$, then we have $\gamma \leq \alpha + \beta$ holds.

Proof:

Similar to the proof of Lemma C.1, we put all vectors on the unit sphere S . Select proper \mathbf{n}_1 and \mathbf{n}_2 directions to ensure that $\mathbf{n}_1 \cdot \mathbf{n}_2 \geq 0$.

In case $\mathbf{n}_2 \cdot \mathbf{n}_3 \geq 0$, as shown in Figure 14 (middle), we have $\angle(\mathbf{n}_2, \mathbf{n}_3) = \pi/2 - \beta$. From Lemma C.1, we know that:

$$\angle(\mathbf{n}_1, \mathbf{n}_3) \leq \angle(\mathbf{n}_1, \mathbf{n}_2) + \angle(\mathbf{n}_2, \mathbf{n}_3) = \pi/2 + \alpha - \beta,$$

$$\angle(\mathbf{n}_1, \mathbf{n}_3) \geq \angle(\mathbf{n}_2, \mathbf{n}_3) - \angle(\mathbf{n}_1, \mathbf{n}_2) = \pi/2 - \alpha - \beta.$$

Thus we have $\gamma = \angle(T_1, \mathbf{n}_3) \leq \alpha + \beta$ holds.

In case $\mathbf{n}_2 \cdot \mathbf{n}_3 \leq 0$, as shown in Figure 14 (right), we have $\angle(\mathbf{n}_2, \mathbf{n}_3) = \pi/2 + \beta$. Similarly we also have $\gamma = \angle(T_1, \mathbf{n}_3) \leq \alpha + \beta$. ■

REFERENCES

- [1] M. Belkin, J. Sun, and Y. Wang, "Constructing Laplace operator from point clouds in \mathbb{R}^d ," in *Proceedings of the 19th Annual ACM-SIAM Symposium on Discrete Algorithms*. Philadelphia, PA, USA: Society for Industrial and Applied Mathematics, 2009, pp. 1031–1040.
- [2] H. Zhang, O. van Kaick, and R. Dyer, "Spectral methods for mesh processing and analysis," in *Proceedings of Eurographics State-of-the-art Report*, 2007, pp. 1–22.
- [3] S. Rosenberg, *The Laplacian on a Riemannian Manifold: An Introduction to Analysis on Manifolds*, ser. London Mathematical Society Student Texts. Cambridge University Press, 1997.
- [4] M. Reuter, F.-E. Wolter, and N. Peinecke, "Laplace-Beltrami spectra as "shape-DNA" of surfaces and solids," *Computer-Aided Design*, vol. 38, no. 4, pp. 342–366, 2006.
- [5] B. Vallet and B. Lévy, "Spectral geometry processing with manifold harmonics," *Computer Graphics Forum*, vol. 27, no. 2, pp. 251–260, 2008.
- [6] B. Lévy, "Laplace-Beltrami eigenfunctions towards an algorithm that "understands" geometry," *Shape Modeling and Applications, International Conference on*, vol. 0, p. 13, 2006.
- [7] L. Miao, J. Huang, X. Liu, H. Bao, Q. Peng, and B. Guo, "Computing variation modes for point set surfaces," in *Point-Based Graphics, 2005. Eurographics/IEEE VGTC Symposium Proceedings*, June 2005, pp. 63–69.
- [8] G. Taubin, "A signal processing approach to fair surface design," in *Proceedings of SIGGRAPH'95*. New York, NY, USA: ACM, 1995, pp. 351–358.
- [9] R. Liu and H. Zhang, "Mesh segmentation via spectral embedding and contour analysis," *Computer Graphics Forum*, vol. 26, pp. 385–394, 2007.
- [10] Z. Karni and C. Gotsman, "Spectral compression of mesh geometry," in *Proceedings of SIGGRAPH'00*, 2000, pp. 279–286.
- [11] D. Cotting, T. Weyrich, M. Pauly, and M. Gross, "Robust watermarking of point-sampled geometry," in *Proceedings of the Shape Modeling International*, 2004, pp. 233–242.
- [12] J. Wu and L. Kobbelt, "Efficient spectral watermarking of large meshes with orthogonal basis functions," *The Visual Computer*, vol. 21, no. 8–10, pp. 848–857, 2005.
- [13] S. Dong, P.-T. Bremer, M. Garland, V. Pascucci, and J. C. Hart, "Spectral surface quadrangulation," *ACM Transactions on Graphics*, vol. 25, no. 3, pp. 1057–1066, 2006.
- [14] J. Huang, M. Zhang, J. Ma, X. Liu, L. Kobbelt, and H. Bao, "Spectral quadrangulation with orientation and alignment control," *ACM Transactions on Graphics*, vol. 27, no. 5, p. 147, 2008.
- [15] P. Mullen, Y. Tong, P. Alliez, and M. Desbrun, "Spectral Conformal Parameterization," *Computer Graphics Forum*, vol. 27, pp. 1487–1494, 2008.
- [16] J. Hu and J. Hua, "Salient spectral geometric features for shape matching and retrieval," *The Visual Computer*, vol. 25, no. 5-7, pp. 667–675, 2009.
- [17] M. Desbrun, M. Meyer, P. Schröder, and A. H. Barr, "Implicit fairing of irregular meshes using diffusion and curvature flow," in *Proceedings of SIGGRAPH'99*. New York, NY, USA: ACM Press/Addison-Wesley Publishing Co., 1999, pp. 317–324.
- [18] M. Meyer, M. Desbrun, P. Schröder, and A. Barr, "Discrete differential-geometry operator for triangulated 2-manifolds," in *Proceedings of Visual Mathematics'02*, 2002.
- [19] G. Xu, "Discrete Laplace-Beltrami operators and their convergence," *Computer Aided Geometric Design*, vol. 21, no. 8, pp. 767–784, 2004.
- [20] U. Pinkall and K. Polthier, "Computing discrete minimal surfaces and their conjugates," *Experimental Mathematics*, vol. 2, no. 1, pp. 15–36, 1993.
- [21] K. Hildebrandt, K. Polthier, and M. Wardetzky, "On the convergence of metric and geometric properties of polyhedral surfaces," *Geometriae Dedicata*, vol. 123, no. 1, pp. 89–112, 2006.
- [22] M. Wardetzky, S. Mathur, F. Kälberer, and E. Grinspun, "Discrete laplace operators: no free lunch," in *Proceedings of the 5th Eurographics Symposium on Geometry Processing*. Aire-la-Ville, Switzerland, Switzerland: Eurographics Association, 2007, pp. 33–37.
- [23] M. Reuter, S. Biasotti, D. Giorgi, G. Patan, and M. Spagnuolo, "Discrete laplace-beltrami operators for shape analysis and segmentation," *Computers & Graphics*, vol. 33, no. 3, pp. 381 – 390, 2009, IEEE International Conference on Shape Modelling and Applications 2009.
- [24] M. Belkin and P. Niyogi, "Towards a theoretical foundation for Laplacian-based manifold methods," in *Lecture Notes on Computer Science*. Springer-Verlag, 2005, vol. 3559/2005, pp. 486–500.
- [25] M. Belkin, J. Sun, and Y. Wang, "Discrete Laplace operator on meshed surfaces," in *Proceedings of the 24th Annual Symposium on Computational Geometry*. New York, NY, USA: ACM, 2008, pp. 278–287.
- [26] R. R. Coifman and S. Lafon, "Diffusion maps," *Applied and Computational Harmonic Analysis*, vol. 21, no. 1, pp. 5 – 30, 2006, Diffusion Maps and Wavelets.
- [27] H. Zhang, "Discrete combinatorial laplacian operators for digital geometry processing," in *Proceedings of SIAM Conference on Geometric Design and Computing*. Nashboro Press, 2004, pp. 575–592.
- [28] C. Luo, J. Sun, and Y. Wang, "Integral estimation from point cloud in \mathbb{R}^d : a geometric view," 2009, to appear in SoCG 2009: Annual Symposium on Computational Geometry.
- [29] N. Amenta, M. Bern, and M. Kamvysselis, "A new Voronoi-based surface reconstruction algorithm," in *Proceedings of SIGGRAPH'98*. New York, NY, USA: ACM, 1998, pp. 415–421.
- [30] N. Amenta and M. Bern, "Surface reconstruction by Voronoi filtering," in *Proceedings of the 14th Annual Symposium on Computational Geometry*. New York, NY, USA: ACM, 1998, pp. 39–48.
- [31] B. Guo, "Surface reconstruction: from points to splines," *Computer-Aided Design*, vol. 29, no. 4, pp. 269–277, 1997.
- [32] J. Giesen and U. Wagner, "Shape dimension and intrinsic metric from samples of manifolds with high co-dimension," in *Proceedings of the 19th Annual Symposium on Computational Geometry*. New York, NY, USA: ACM, 2003, pp. 329–337.
- [33] S. Har-Peled and K. Varadarajan, "Projective clustering in high dimensions using core-sets," in *Proceedings of the 18th Annual Symposium on Computational Geometry*. New York, NY, USA: ACM, 2002, pp. 312–318.